An efficient hybrid advection scheme in a level set framework coupling WENO5 and HOUC5 schemes based on kink detection

Félix Henri, Mathieu Coquerelle, Pierre Lubin

An efficient hybrid advection scheme in a level set framework coupling WENO5 and HOUC5 schemes based on kink detection

Félix Henri*, Mathieu Coquerelle*, Pierre Lubin*

Bordeaux INP, I2M, UMR 5295, F-33400 Talence, France.

Abstract

We present a novel robust, accurate and efficient hybrid strategy by coupling WENO5 and HOUC5 schemes for the spatial discretization of the advection equation in a level set framework. This one is based on two main observations. First, from its definition, the level set function is globally a smooth function in the whole domain except where kink points are detected. And secondly, for smooth regions, the 5^{th} order Weighted Essentially Non-Oscillatory (WENO5) scheme reduces to compute a 5^{th} order High-Order Upstream Central (HOUC5) scheme, which has a lower computational cost. The introduced hybrid scheme HWH5, for hybrid WENO5 scheme HOUC5 scheme, coupled the robustness of a WENO5 scheme for all regions where the spatial discretization of the advection equation is subject to large error, i.e. where a kink is detected, with the efficiency of a HOUC5 scheme for smooth regions. The efficiency and robustness of this approach are demonstrated on a variety of benchmarks, where the hybrid approach presents equivalent results to the WENO5 scheme for a computational cost lowered with a factor up to 2.

Alongside, we also present that the sole use of the efficient HOUC5 scheme for the spatial discretization of the advection equation presents anti-diffusive behaviours on the volume conservation and may lead to the introduction of noticeable perturbations of the interface which can be dreadful overtime on the overall dynamic. Conversely, WENO5 presents diffusive results in irregular regions. Hence, the adequate coupling of these two schemes in HWH5 allows obtaining a method as robust as WENO5 for a valuable lowered computational cost.

Keywords: level set method, hybrid advection scheme, WENO schemes, HOUC schemes, conservative advection equation, kink detection

*Corresponding Author

Email addresses: felix.henri@u-bordeaux.fr (Félix Henri), mathieu.coquerelle@bordeaux-inp.fr (Mathieu Coquerelle), pierre.lubin@bordeaux-inp.fr (Pierre Lubin)

Highlights

- Hybrid spatial scheme for solving the advection equation in a level set framework.
- Straightforward implementation of the hybrid approach.
- Numerical cost reduced, up to 50%, compared to WENO5 for the same robustness and accuracy.
- Comparative study of diffusive and anti-diffusive matters of numerical schemes.

1. Introduction

The accurate representation of an evolving geometrical surface is essential in many applications. In multiphase flows, it requires adequate numerical methods for localizing precisely each phase and their interactions at the interface such as buoyancy and surface tension. The dynamics of such interfaces can be relatively complex as they are subjected to high velocity gradients, shear as well as topology changes.

For this purpose, the Level Set method [1] (LSM) is a popular approach to represent evolving interfaces. It captures the interface as the iso-surface of a scalar function which is usually defined as a signed distance function. Using this implicit definition, topology changes are naturally handled and the interface properties, such as the normal and curvature, can be easily and accurately calculated. However, this method suffers from difficulties, particularly regarding mass conservation. This problem arises from two main reasons: first, from the transport of the level set where the discretization of the advection equation inevitably introduces numerical errors and, secondly, during the frequent reinitialization procedure [2–4] used to reshape the level set as a signed distance function, wherein the interface position can be altered, also because of numerical errors. The problems of mass conservation for LSM have been one of the principal subjects of research over the past years. Many strategies have been explored for the improvement of advection and reinitialization, as well the level set representation itself or the use of coupled methods. We steer the reader to the work of [5, 6] for a detailed review of the literature.

As mentioned above and made evident in many works [6, 7], the use of high-order schemes is essential for accuracy and robustness since it will not only impact the mass conservation, but also the fidelity of the transported interface and the accurate computation of associated geometric properties such as curvature. One of the most popular choices for the spatial discretization of the advection equation is the 5^{th} order Weighted Essentially Non-Oscillatory (WENO) scheme [8], initially for treating shocks in compressible flows. It is based on a combination of 3^{rd} order interpolation schemes through non-linear weights; it optimally converges to 5^{th} order accuracy in smooth regions and decreases to 3^{rd} order close to a discontinuity, with much reduced oscillations. It is particularly suited for LSM where the scalar function can attain high gradients or where its derivative is discontinuous, i.e. near kinks [4].

An alternative and more efficient approach is the High-Order Upstream Central (HOUC) scheme introduced in [7]. In contrast to the WENO scheme, it is based on Lagrangian polynomials and thus linear weights. However, it has low accuracy in non-smooth regions and can lead to important numerical oscillations near discontinuities. The justification of using HOUC for LSM relies on the fact that, from its definition, the level set field is and should remain globally a smooth function almost everywhere, and particularly close to the interface. Consequently, using non-linear non-oscillatory schemes should not be necessary unless the function deviates from a smooth function.

When incompressible flows are considered, another approach has recently been proposed [6, 9–12] based on the rewriting of the advection equation in a conservative form with an adapted WENO scheme.

This paper focuses on the discretization of the level set advection with the three different strategies described above. For simplicity and clarity, WENO5 and HOUC5 will be referred to as, respectively, the use of the 5^{th} order WENO and HOUC scheme when the non-conservative form of the advection equation is considered. While WENO5cons will denote the use of the modified 5^{th} order WENO scheme applied to the conservative form of the advection equation.

We will first demonstrate on a simple case that, when coupled with a reinitialization procedure, HOUC5 and the conservative WENO5 can present anti-diffusive behaviour on the volume conservation thus leading

to undesired perturbation of the interface. On the contrary, the non-conservative WENO5 presents diffusive behaviours which we believe to be more stable for complex two-phase flow simulations. These observations will be corroborated in the various benchmarks of the result section.

Finally, a novel robust and efficient hybrid scheme (HWH5) is introduced. The main objective is to retain the same accuracy and dissipative behaviour of the WENO5 scheme close to non-smooth regions while globally reducing the computational cost thanks to the use of the HOUC5 scheme everywhere else. The strategy relies on the efficient detection of kinks, enhancing the initial algorithm presented in [4]. The efficiency and robustness of this approach are demonstrated on a variety of benchmarks, where the hybrid approach leads to equivalent results as the WENO5 scheme for a computational cost lowered up to 50%.

2. The Level Set Method coupled with Navier-Stokes equations

2.1. Level set definition

Let consider a spatial domain Ω, composed by two subdomains Ω^- and Ω^+ separated by an interface Γ. For immiscible two-phase flow problems, Ω^- and Ω^+ locate each phase and Γ the interface between them. In a level set framework, Γ is represented implicitly by a scalar function $\phi : \Omega \to \mathbf{R}$ which is defined as a signed distance function:

$$\phi(\mathbf{x}) = \begin{cases} -\text{dist}(\mathbf{x}, \Gamma) \text{ if } \mathbf{x} \in \Omega^- \\ +\text{dist}(\mathbf{x}, \Gamma) \text{ if } \mathbf{x} \in \Omega^+ \end{cases} \tag{1}$$

where $\text{dist}(\mathbf{x}, \Gamma)$ is the Euclidean distance of $\mathbf{x}$ to the interface. Consequently, the interface is defined by the zero level set of ϕ:

$$\Gamma = \{\mathbf{x} \in \Omega \mid \phi(\mathbf{x}) = 0\}.$$

Furthermore, in that particular case, ϕ is solution of the eikonal equation :

$$\|\nabla\phi\| = 1. \tag{2}$$

2.2. Navier-Stokes equations for incompressible two-phase flows

We considered the incompressible form of the Navier-Stokes equation where the momentum equation can be written in a conservative form as:

$$\frac{\partial \rho \mathbf{u}}{\partial t} + \nabla \cdot (\rho \mathbf{u} \otimes \mathbf{u}) = -\nabla p + \nabla \cdot (2\mu \mathbf{D}) + \mathbf{f}$$

where $\mathbf{u}$ is the fluid velocity, ρ its density, μ its dynamic viscosity, p the pressure, $\mathbf{D} = (\nabla \mathbf{u} + \nabla \mathbf{u}^t)/2$ is the deformation tensor and $\mathbf{f}$ encompasses external body forces such as buoyancy.

Under the assumption of incompressibility, the continuity equation reduces to a divergence-free constraint on the velocity field:

$$\nabla \cdot \mathbf{u} = 0$$

In the case of an immiscible two-phase flow, the density and viscosity fields are discontinuous, a matter that can be treated following the one fluid model, first introduced in [13].
In the case where the density and viscosity are constant within each phase, ρ and μ are expressed as:

$$\begin{aligned} \rho(\mathbf{x}) &= \rho_2 + (\rho_1 - \rho_2) c(\mathbf{x}) \\ \mu(\mathbf{x}) &= \mu_2 + (\mu_1 - \mu_2) c(\mathbf{x}) \end{aligned} \tag{3}$$

where ρ_1 (resp. ρ_2) and μ_1 (resp. μ_2) are the values of the first (resp. second) phase and c a characteristic function, also referred as the volume fraction.

Level set coupling. In a level set framework, c is expressed as a function of ϕ. In order to obtain a smooth representation of the interfacial region, a regularized form of the Heaviside function is used:

$$c(\mathbf{x}) = H_\epsilon(\phi(\mathbf{x})) \quad \text{with} \quad H_\epsilon(\phi) = \begin{cases} 0 & \text{if} \quad \phi < \epsilon \\ \frac{1}{2}\left(1 + \frac{\phi}{\epsilon} + \frac{1}{\pi}\sin\left(\phi\frac{\phi}{\epsilon}\right)\right) & \text{if} \quad |\phi| \leq \epsilon. \\ 1 & \text{if} \quad \phi > \epsilon \end{cases} \tag{4}$$

Hence, the density and viscosity vary smoothly within the interfacial region of thickness $2\epsilon = 2kh$ centered around Γ, where h is the cell size and k a constant (usually between 1.5 and 3). Sharper approaches for approximating the volume fraction could also be used, but this topic is outside of the scope of this article.

2.2.1. Surface tension model

Surface tension can be modeled as a pressure jump across the interface from a volume point of view as $\mathbf{f}_\sigma = \sigma\kappa_\Gamma\mathbf{n}_\Gamma\delta_\Gamma$, where σ is the surface tension coefficient, κ_Γ the curvature of the surface and $\mathbf{n}_\Gamma$ its normal and δ_Γ is the Dirac function associated to the surface. Brackbill et al. [14] introduced the Continuum Surface Force (CSF) which approximates surface tension as a body force:

$$\sigma\kappa\mathbf{n}\delta_\Gamma \simeq \sigma\kappa\nabla c. \tag{5}$$

Using the level set formulation, the normal $\mathbf{n}$ and the curvature κ associated to the interface can be expressed as:

$$\mathbf{n} = \frac{\nabla\phi}{\|\nabla\phi\|} \quad \text{and} \quad \kappa = \nabla\cdot\mathbf{n} = \nabla\cdot\left(\frac{\nabla\phi}{\|\nabla\phi\|}\right).$$

2.3. Level set transport

The interface position evolves over time by solving the advection/transport equation applied to the level sets in a Eulerian framework:

$$\frac{\partial\phi}{\partial t} + \mathbf{u}\cdot\nabla\phi = 0 \tag{6}$$

where $\mathbf{u}$ is the underlying velocity field.

In a general case, solving eq. (6), will stretch and compress level sets of ϕ which will then cease to be a signed distance function. This problem is remedied by applying the reinitialization algorithm, where the level set scalar field is reconstructed in a way to satisfy the eikonal equation eq. (2) without altering the interface position.

2.4. Level set reinitialization

In this work, the reinitialization procedure is performed using the widely used method based on solving a partial differential equation (PDE) [2, 3, 15, 16], where a front is propagated in the normal direction from the interface by solving a PDE, which derives from the Hamilton-Jacobi equation, over a fictitious time τ:

$$\frac{\partial\psi}{\partial\tau} + \mathrm{sgn}(\psi_0)(\|\nabla\psi\| - 1) = 0 \quad \text{with} \quad \psi_0 \equiv \psi(\tau = 0) = \phi. \tag{7}$$

The complete reinitialization of the level set function is the stationary solution of eq. (7). In the following sections, eq. (7) will be referred to as the H-J equation.

3. Spatial discretization for the transport equation

As introduced above, the interface position is transported implicitly by solving the advection equation eq. (6). The accurate and robust resolution of this latter is essential for volume conservation and in order to avoid the introduction of perturbations in ϕ and its derivatives of higher degree which will, for instance, perturb the curvature computation and consequently surface tension. Hence, adequate numerical methods have been developed in order to achieve these goals.

In the literature, the advection equation can be found in two different forms: the first one, as defined earlier in eq. (6), will be referred to as the *classical advection equation*. Secondly, in the case where the velocity field is divergence-free, eq. (6) can be algebraically rewritten in a conservative form, detailed in section 3.3, and referred to as the *conservative advection equation*.

$\frac{\partial \phi}{\partial t} + \mathbf{u} \cdot \nabla \phi = 0$	Classical advection equation
$\frac{\partial \phi}{\partial t} + \nabla \cdot (\mathbf{u}\phi) = 0$	Conservative advection equation

3.1. Temporal integration

For both equations, temporal integration can be done using several strategies such as the Adams-Bashforth method [17] or a Non-Strong Stability Preserving explicit Runge-Kutta method (RK-NSSP) [18]. As they have been widely studied, these methods will be not detailed further and, in the entire document, all results have been obtained using a 2^{nd} order RK-NSSP 3,2 scheme.

3.2. Spatial discretization of the classical advection equation

The spatial discretization of the classical advection equation complexity lies in the accurate computation approximation of $\nabla\phi$. This can be done by various spatial schemes such as Weighted-Essentially-Non-Oscillatory (WENO) schemes [8] or High-Order Upstream Central (HOUC) schemes [7]. Anyhow, the algorithm can be solved simultaneously and independently for all 3 directions (in 3D), given adequate formulation, and we will thus focus the following section on 1D schemes.

3.2.1. WENO schemes

A popular choice to compute $\nabla\phi$ is the WENO 5,3 scheme (denoted as WENO5). The main advantages of this scheme are its robustness and accuracy through its non-linear formulation. Theoretically, it converges to 5^{th} order in smooth regions and is also non-oscillatory in the presence of a discontinuity, by locally reducing to 3^{rd} order precision. Hence this scheme is particularly suitable to avoid introducing any perturbations on ϕ, its derivatives of higher degree and particularly when computing the curvature.

An upwind approximation ϕ_x^- of the first derivative of ϕ at a point (x_i) using WENO5 can be summarized as a weighted combination of three 3^{rd} order approximations:

$$\phi_x^-(x_i) = \sum_{k=1}^{3} w_k \left(IS_k\right) \phi_x^{-,k}(x_i)$$

where $\phi_x^{-,k}(x_i)$ are the 3^{rd} order approximations of ϕ_x on the associated sub-stencils $S_k = \{x_l \mid l = i+k-3, ..., i+k\}$ for $k = \{1, 2, 3\}$ and w_k are the associated non-linear weights. The downwind scheme $\phi_x^+(x_i)$ is constructed in a symmetrical manner. When ϕ is smooth, the weights coincide with the weights of the optimal 5^{th} order scheme, i.e. the HOUC5 scheme (see next section). However, when ϕ is not smooth, the weights are modified such as if a stencil contains a discontinuity, its influence is diminished, i.e. its weights tend to zero.

In order to do so, the smoothness indicators IS_k evaluate the smoothness of ϕ inside each stencil. Numerically, the smoothness indicators are evaluated as the sum of derivatives of the interpolation polynomial and are hence themselves a non-linear combination of discrete values of ϕ.

The computation of the non-linear weights via smoothness indicators combined with 3^{rd} order approximations make the WENO5 approximation robust and accurate but expensive. However, as pointed out by Nourgaliev et al. (fig. 17 of [7]), in practice, as smoothness indicators will not be always equal with level set fields, even far from kinks, the scheme will be sub-optimal, i.e. with and accuracy between third and fifth order.

A variety of approaches exist for the construction of WENO schemes. All methods have a common base: a weighted combination of numerical schemes evaluated on different stencils, the calculation of weights (w_k) and smoothness indicators (IS_k) have been studied in several researches, as for example in [19–21]. In the article, we chose WENO-Z5,3 scheme of [21] which shows a reasonable compromise between computational cost and accuracy. An efficient implementation of the scheme is described in section A.

3.2.2. HOUC5 scheme

As introduced before, an alternative approach has been presented in [7] as the High-Order Upstream Central (HOUC) scheme. It relies on the observation that the level set field is, and should remain, globally a smooth function and, consequently, using usual non-linear essentially non-oscillatory schemes (e.g. WENO5) is not necessary. Hence, [7] proposed to replace the usual WENO5 scheme with the associated Lagrange interpolation scheme, i.e. the HOUC5 scheme, which is more efficient without any detriment to numerical stability and accuracy.

The upwind 5^{th} order HOUC approximation of ϕ_x^- at a point (x_i) is given by:

$$\phi_x^-(x_i) = \frac{1}{60}(-2\phi_{i-3,j} + 15\phi_{i-2,j} - 60\phi_{i-1,j} + 20\phi_{i,j} + 30\phi_{i+1,j} - 3\phi_{i+2,j}). \tag{8}$$

The construction of ϕ_x^+ is obtained symmetrically.

Comparatively to a WENO5 scheme, the HOUC5 scheme is of much lower computational cost but is not non-oscillatory. As demonstrated in the various benchmarks of [7], the HOUC5 scheme is sufficiently dissipative to ensure the overall stability of the solution in the presence of corners where the first derivatives of the level set function are not defined and hence close to kinks. However, we will demonstrate in the next section that it may exhibit undesired behaviour for capturing the interface, particularly close to under-resolved regions.

3.3. Spatial discretization of the conservative advection equation

When considering incompressible flows, another strategy consists in rewriting the classical advection equation eq. (6) in a conservative form as:

$$\frac{\partial \phi}{\partial t} + \nabla \cdot (\mathbf{u}\phi) = 0 \tag{9}$$

since $\nabla \cdot (\mathbf{u}\phi) = \mathbf{u} \cdot \nabla\phi + (\nabla \cdot \mathbf{u})\phi$ and $\nabla \cdot \mathbf{u} = 0$.

The term $\nabla \cdot (\mathbf{u}\phi)$ is discretized using a modified WENO5 scheme adapted to compute the advection term in its conservative form, based on cell-mean values of ϕ as in a finite volume approach. This method is called the *modified WENO5* or *conservative WENO5* in the literature, depending on the authors. Herein, for convenience, it will be referred to as *WENO5cons*. Since the construction of this scheme follows the same idea as the finite differences WENO5 scheme described above, further details will not be given but can be found in [6].

It should be stressed that, in our context, all results using the WENO5cons method have been done for a level set defined as a signed distance function (as in [6, 9–12]). A different and alternative approach, also

named "conservative level set", where the field ϕ is defined through a hyperbolic tangent function [22, 23] is not the subject of our work and thus will not be treated here.

4. Study of the anti-diffusivity of the HOUC5 and WENO5Cons schemes for level set advection

In this section, through 1D and 2D illustrative cases, we will show that both HOUC5 and WENO5cons schemes can reveal anti-diffusive behaviours on volume conservation which can introduce unwanted perturbations of the interface. On the contrary, non-conservative WENO5 exhibits diffusive behaviour in the vicinity of under-resolved regions. Those observations agree with the recent comparative study of [6]. More precisely, as it will be presented below, this behaviour arises from the spreading of level sets close to kink points by HOUC5 and WENO5cons schemes when using a frequent reinitialization procedure.

First, the problem will be illustrated on the single vortex 2D case which is widely used as a key test for interface methods. Then, we will propose an explanation for this issue emergence, particularly when coupled to the H-J reinitialization algorithm. Further examples will also be given in the results section section 7 to complete our observations.

4.1. 2D advection: single vortex

In the single vortex 2D case (see sec. 7.6 for details), the interface is first stretched in order to create a thin filament and then, with the flow reversed, the initial disk should be recovered. However, due to numerical errors, the interface may fail to return to its original circular shape. The main difficulty arises during the stretching step when the interface will become thinner and thinner to a point that the tip of the tail will fall below grid resolution, and hence discrete Eulerian schemes will fail to capture it correctly. As depicted in fig. 1 for an intermediate and representative mesh, at that moment of the stretching step, two distinct behaviors occur. The WENO5 scheme will have a diffuse nature, making the thin interface shrink and thus leading to a loss of the shape's total volume. On the contrary, both HOUC5 and WENO5cons have an anti-diffuse behavior that enlarges the tail.

In this configuration, even if the enlargement of the tail is moderate it can induce perturbations over time. As illustrated in figure fig. 2, when $t = T$ both the HOUC5 and WENO5cons returned to a shape that is clearly perturbed around the top, even though the total volume seems well conserved. In contrast, the WENO5 scheme helps the interface returning to a smoother shape, which, for typical fluid flow simulations, better corresponds to a physical solution thanks (and despite) to higher diffusion.

These two opposite behaviors are not only occurring on the particular single vortex case but are also observable in many others, as we will see in the results section section 7.

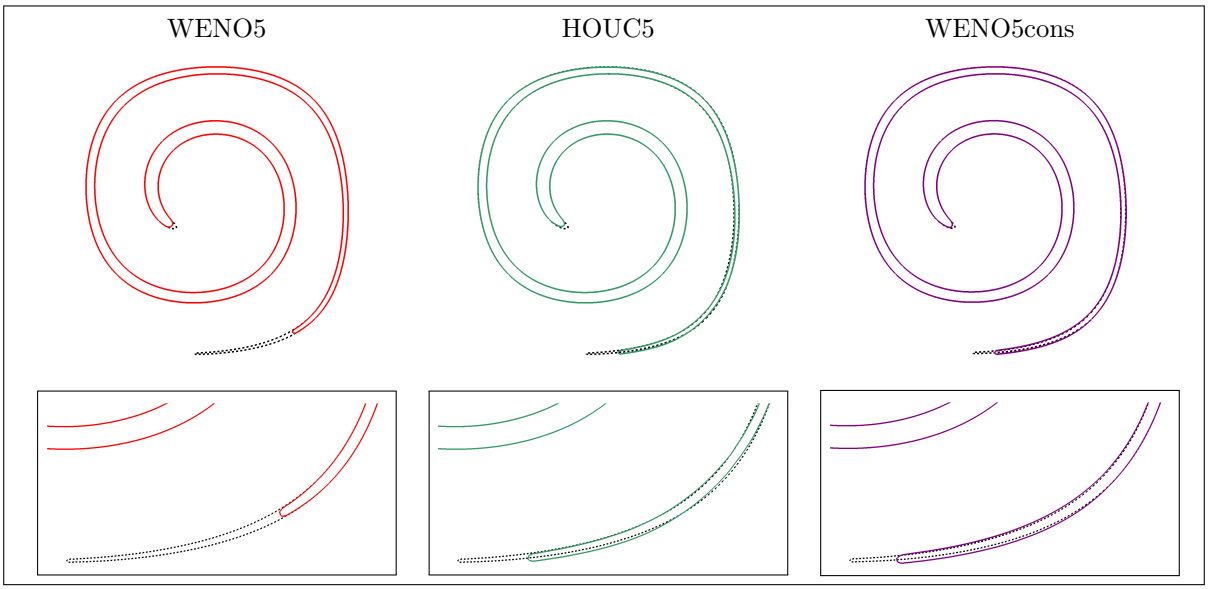

Figure 1: Interface shape for the single vortex test case at maximal deformation $t = T/2$ when $T = 8.0$ at a mesh resolution of 128^2 cells. On the top the full view of the shape, on the bottom a zoom of the trailing of the tail. The reference solution, obtain using a WENO5 scheme at a mesh resolution of 1024^2 cells, is drawn with black dashed lines. Reinitialization is performed as described in sec. 7.2.2.

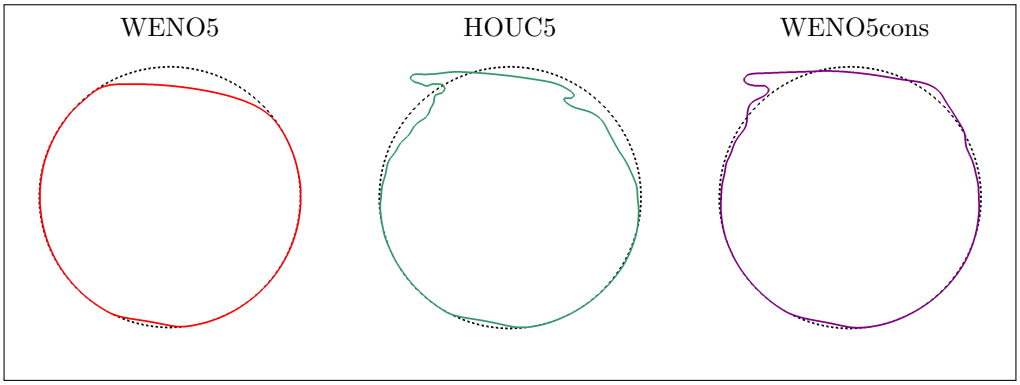

Figure 2: Interface shape for the single vortex test case at reverse time $t = T$ when $T = 8.0$ at a mesh resolution of 128^2 cells. The reference solution, is drawn with black dashed lines. Reinitialization is performed as described in sec. 7.2.2.

4.2. 1D advection

The enlargement or shrink problem observed in the tail of the interface in the previous section can be further studied by considering a 1D advection case. On a $[0, 1]$ domain, with a resolution of 32^2 cells, the interface is initialized at points $0.5 - 1.75\Delta x$ and $0.5 + 1.75\Delta x$. This is equivalent to consider a phase centered in the domain with a width of $3.5\Delta x$. Periodic boundary conditions are set on the limits of the domain and the velocity field is set to $U = 1$. Hence, with a time step of $\Delta t = 0.005$, the interface returns to its original position after 200 advection steps.

fig. 3 shows the results using the three studied schemes. Comparatively to the expected solution in gray dashed line, after 200 advection steps without any reinitialization (left subfigure), we observe that the use of either HOUC5 or WENO5cons schemes tend to spread the solution of the level set close to the kink while WENO5 tends to diffuse the solution. This concurs with the statement given regarding the 2D case. After

applying the reinitialization procedure after this 200^{th} step (center figure), it results for both HOUC5 and WENO5cons an enlargement of the level set solution compared to the exact solution and consequently an increase of the volume of that phase. This contrasts with the use of the WENO5 scheme which has a diffusive behaviour on the sharp shape of the level set, i.e. at the kink. Consequently, after the reinitialization step the volume locally diminishes.

The reinitialization procedure was here applied after a large number of advection steps in order to depict separately the consequences of the advection scheme. However, in practical use, the reinitialization procedure is applied more frequently (around every 10 advection steps, or when the level set field is too much deformed, depending on the flow field). The last subfigures depict that, in that case, closer to real usage, the same problem arises and is even more noticeable.

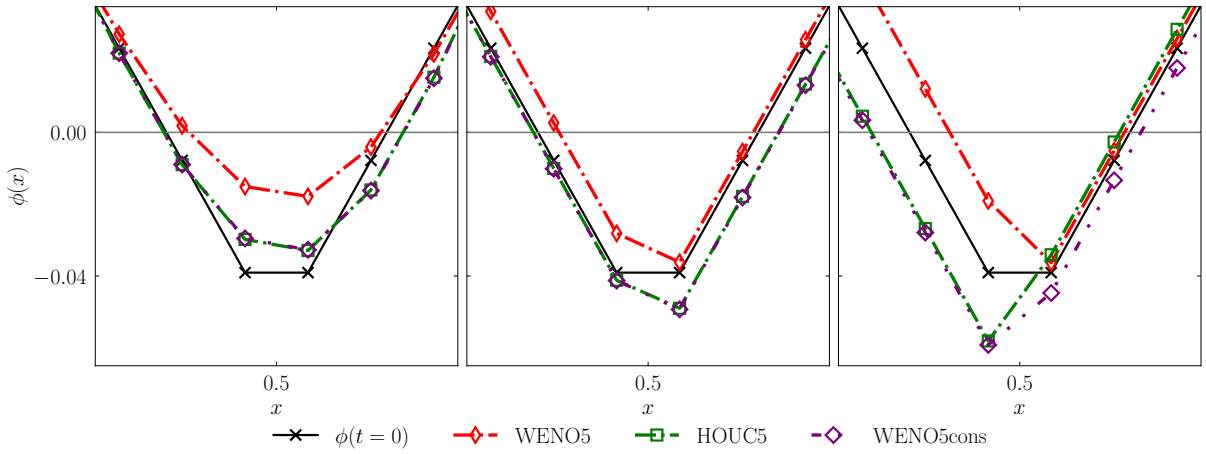

Figure 3: Numerical result of the advection 1D of the level set at a time $t = 1.0$ which corresponds to 200 advection step performed. Left: result without any reinitialization step. Middle: result when only one reinitialization procedure is applied at $t = 1.0$. Right: result when the reinitialization procedure is applied every 10 advection steps.

4.3. Discussion on volume gain and loss and potential induced perturbations

To conclude, it is arduous and delicate to state whether it is preferable to use an interface method with diffusive or anti-diffusive behavior. In some particular cases, as presented in [6, 7], having an anti-diffusive scheme can result in a better small structures volume conservation and hence, the choice between the strategies will surely depends on the final application.

However, as presented in this section and in the following test cases (in particular, see section sec. 7.4, 7.6 and 7.8), an anti-diffusive behavior can introduce non-negligible perturbations on the interface, and particularly close to small structures and kinks. In some cases, it could be possible that these perturbations can sufficiently disturb the interface to a point leading to the emergence of topology changes where there should not be any. This matter could be critical, for example, in some complex two-phase flows, like for atomization application, by introducing erroneous interface rupture or, when considering breaking waves, by introducing surface instabilities. Consequently, even if this subject will remain an open question, we esteem that using a diffusive property is more suitable in most of the cases and thus, particularly near kinks, a non-conservative WENO5 scheme should be employed.

5. Hybrid scheme for the advection equation

In this section we will introduce a novel hybrid approach, referred to as HWH5, which takes the advantages of the accuracy and robustness of the WENO5 scheme and the efficiency of the HOUC5 scheme. This latter arise from the same observation as [7]: for smooth regions, the non-linearity of the WENO5 scheme is not needed since there is no large values in ϕ derivatives, and hence a HOUC5 scheme is more suitable. This

latter assumption is reinforced by the property that, when all WENO5 smoothness indicators (i.e. IS_k) are equal, which is the case for smooth regions, the WENO5 scheme is mathematically equal to the HOUC5 scheme. However, as demonstrated in the previous section, applying the HOUC5 scheme at all points, as in [7], can introduce undesired perturbations, and particularly close to kinks. In order to avoid these important numerical errors, the hybrid scheme is constructed to use a HOUC5 scheme where the level set is trustfully smooth and a WENO5 scheme otherwise. Furthermore, this hybrid method ensure to always used a 5^{th} order scheme for smooth regions thanks to the use of a HOUC scheme, which is not always the case for a WENO5 scheme as presented in [7].

Hence, this novel strategy relies on the fast and accurate detection of *trustworthy* points which will be used to choose between each scheme. We thus expect a noticeable gain in computational time, under the assumption that the overhead cost of detecting these regions is lower than the latter. It is noticeable that this strategy could work for any scalar field, as soon as it is possible to detect all ill-defined regions where the use of a robust non-linear scheme is required. In the particular case of level set methods, these points are defined as the kink points, as described below.

5.1. Kink detection

In the case of a level set defined as a signed distance function, the overall field is globally smooth excepted on particular points, defined as kinks, where the computation of the derivatives of ϕ will be miscalculated and will induce large perturbations in the solution, and, more importantly, on the interface. We distinguish two types of kinks, as detailed in [4]:

- inherent kinks: points that are part of the medial axis, as part of the level set representation and where the derivatives of ϕ are not defined [4, 24, 25];
- numerical kinks: points that are not part of the medial axis and that appear because of numerical errors, after topological changes or near under-resolved regions [4].

The detection of all the cells containing a kink, where the set of these cells is noted Ω^K is done using the kink detection algorithm of Henri et al. [4]. Details of the algorithm and efficient implementation are given in sec. 6.1.

Difference between the kink detection and computation of the IS_k. The main difference between using a kink detector rather than using the smoothness indicators IS_k, is that we compute a global map locating stencils that will certainly induce large errors on the computation of derivatives of ϕ if at least one kink is present. Rather than computing multiple IS_k (three per direction in the case of the WENO5), which moreover are non-linear, we can benefit from knowing precisely which cells should be treated with care.

Hence, even if this approach adds an overhead computational cost for detecting kinks, we will show in the results section (see section 7) that this methodology globally lowers the cost of the advection of the level set.

5.2. The hybrid method

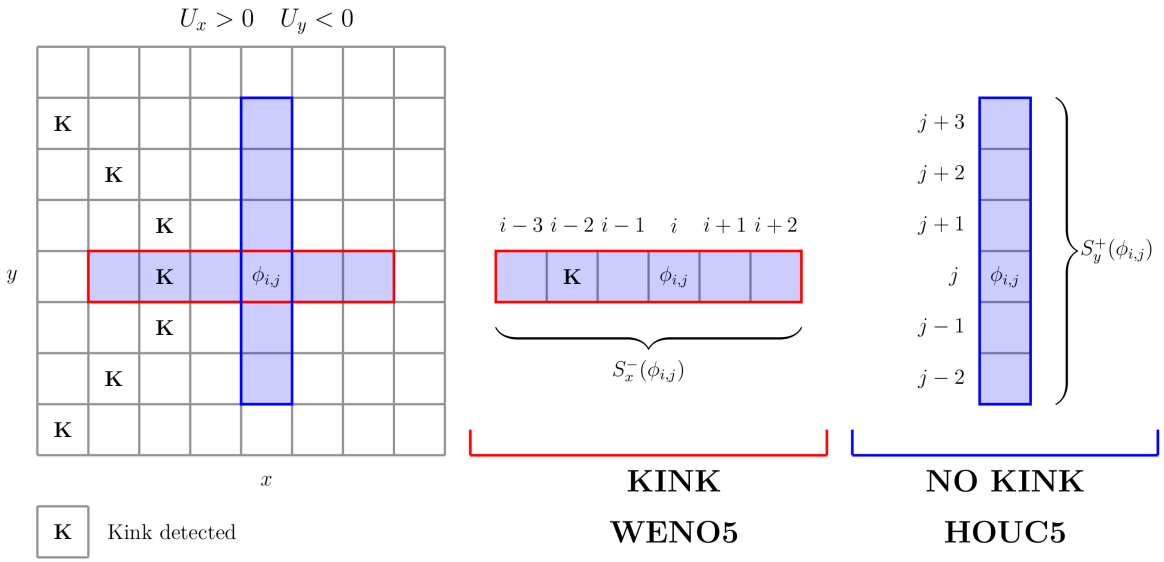

Figure 4: Illustration of the algorithm in 2D for computing $\nabla\phi$. The cells detected as containing a kink are marked with a **K**. In x-direction, for a velocity $U_x > 0$, the stencil $S_x(\phi_{i,j})$ is left off-centred and contains a kink. Hence a WENO5 scheme is used for computing $\partial\phi/\partial x$. In y-direction, $U_y < 0$, thus the stencil $S_y(\phi_{i,j})$ is up off-centred and does not contain a kink. Hence a HOUC5 scheme is used for computing $\partial\phi/\partial y$.

Before solving the advection equation eq. (6), we build the map Ω^K of all cells containing kink points. Then, the computation of the advection term $\mathbf{u}\cdot\nabla\phi$ is done by selecting the appropriate scheme, depending on the presence of kinks in the associated stencils around a cell. We propose a complete and detailed description of the procedure in algorithm 1, as well as an associated illustration of the method in fig. 4. Efficient implementation of the scheme selection process is given in sec. 6.2.

The main purpose of the procedure is to compute the first derivative of ϕ in each direction d (which can be x, y or z, since the procedure is the same for all directions) with the most suitable numerical scheme. This choice depends on the presence of a kink in the scheme's stencil. Let $S_d^{\pm}$ be the set of cells used by the scheme, may it be HOUC5 or WENO5, in accordance with the upwind/downwind direction of the flow. In x-direction, let U_x be the associated velocity, then, if $U_x > 0$ then the associated upwind stencil is: $S_x^+ = \{c_{i+l,j,k} \mid l \in [\![-3,+2]\!]\}$ and, if $U_x < 0$ then the downwind stencil is: $S_x^- = \{c_{i+l,j,k} \mid l \in [\![-2,+3]\!]\}$. Given the stencil, we look if at least one of the cells c_l part of $S_x^{\pm}$ has been marked as containing a kink. If not, we can safely compute $\partial\phi/\partial x$ with the appropriate HOUC5 scheme associated to the stencil $S_d^{\pm}$; otherwise, a WENO5 scheme is used. The exact same process is used for y and z directions. We thus compute the advection term with:

$$(\mathbf{u}\cdot\nabla\phi)_{i,j,k} = \sum_{d\in\{x,y,z\}} U_d \left.\frac{\partial\phi}{\partial d}\right|_{i,j,k}.$$

Algorithm 1: Computation of $(\mathbf{u} \cdot \nabla\phi)_{i,j,k}$ with the hybrid HWH5 method. The kink map Ω^K is given as input.

ugradphi $\leftarrow 0$
for $d \in [x, y, z]$ **do**
  if $U_d > 0$ **then**
    $S_d \leftarrow S_d^-$ ▷ backward scheme stencil
  else if $U_d < 0$ **then**
    $S_d \leftarrow S_d^+$ ▷ forward scheme stencil
  KinkInStencil $\leftarrow$ false
  for $c_{i',j',k'} \in S_d$ **do** ▷ see sec. 6.2 for a more efficient implementation
    if $\Omega^K_{i',j',k'}$ **then**
      KinkInStencil $\leftarrow$ true
      break ▷ at least 1 kink in stencil, leave the loop
    end
  end
  if KinkInStencil **then** ▷ scheme selection
    ugradphi $\leftarrow$ ugradphi $+ U_d \times$ WENO5$(\phi, \mathrm{S_d})$
  else
    ugradphi $\leftarrow$ ugradphi $+ U_d \times$ HOUC5$(\phi, \mathrm{S_d})$
  end
end
Return ugradphi

Updating the kink map. It is important to note that, when the temporal integration is split into several intermediate integration steps, e.g. with a 2^{nd} order Runge-Kutta scheme, a cell can switch from containing a kink to not containing a kink (or inversely), between two intermediates steps. Therefore, a rigorous way would be to update Ω^K between each sub-iteration which would undoubtedly increase the overall computational time. However, in practice, we have observed that this procedure is not strictly required. First, only the case where a cell switches from not containing a kink to containing a kink matter, since in the other case a WENO5 scheme is used. Secondly, this configuration will be occasional due to CFL restriction. And finally, when it will occur, the anti-diffusive behaviour of the HOUC5 will have almost no effects since they are dreadful only accumulated through time and will be compensated by the use of a WENO5 scheme at the next advection step.

In consequence, we have chosen to compute the kink map only once before solving the advection equation and not between each sub-integration step.

6. Details on some numerical implementation

The proposed method requires supplementary work in order to select adequately the advection numerical scheme. Additional procedures, i.e. the kink detection and the test for kinks, should not represent a significant overhead regarding the computational cost, otherwise the gain of using the hybrid scheme would be much less significant. In consequence, we present below efficient implementations of the associated algorithms.

6.1. Efficient kink detection implementation

First, we propose an efficient implementation of the kink detection algorithm given in [4]. A 3D version is given in alg. 2 which results in the array Ω^K, indicating cells that are considered as kinks.

A level set kink is defined as a point where the local field is ill-defined, i.e. either being near a medial axis (inherent kink) or in a non-smooth region (numerical kink). The leading idea of the kink detection algorithm is to search for closest point approximations around a cell's center and evaluate if they do not spread too far away. This process can be reduced and simplified in the comparison of biased normals, where the bias is obtained by off-centering numerical differentiation.

Efficiency is achieved by pre-computing values that are used redundantly, as well as on a heuristic for the normals comparison. Step (I) consists in computing the biased derivatives of $\phi_{i,j,k}$ in each direction and saving them in variables $(D_x^-, D_x^+, D_y^-, D_y^+, D_z^-, D_z^+)$. Then, in step (II), the 8 normals (4 in 2D) corresponding to the 8 vertex directions are trivially generated. Finally, in step (III), normals are compared in order to detect discrepancies in the closest point approximation. Comparing each 28 (6 in 2D) possible pair of normals can become expensive. As the vectors are built on biased derivatives, taking opposite directions that do not share common terms will lead to maximizing the eventual discrepancy in the closest point approximation. Hence, we only effectuate 4 comparisons (2 in 2D) between: $\mathbf{n}^{---}$ / $\mathbf{n}^{+++}$, $\mathbf{n}^{--+}$ / $\mathbf{n}^{++-}$, $\mathbf{n}^{-+-}$ / $\mathbf{n}^{+-+}$ and $\mathbf{n}^{+--}$ / $\mathbf{n}^{-++}$. This represents a substantial reduction of numerical operations, particularly in 3D. This heuristic can also be understood from a geometrical point of view: if the eventual medial axis is a surface or a curve locally, two opposite points will undoubtedly be on each side of that entity and thus will lead to distant closest points.

In practice, performing this approach detects fewer kinks than the original algorithm of [4], a very small difference in proportion. We are confident that less false positives are detected and that, if kinks are missed, they are part of numerical kinks that would eventually be discovered with a smaller threshold or at the next iteration. Nevertheless, we have found that these mere differences did not affect the results presented in section 7. The threshold ϵ used in the comparison of two normals to indicate the presence of a kink is the same as the one used in [4]: i.e. $\epsilon = 1/2$.

Algorithm 2: Efficient kink detection implementation. In practice, in the code, the inner loops are inlined.

$\Omega^K \leftarrow$ false ▷ `Initialize the kink map`
for $i \in N_x$ **do**
  for $j \in N_y$ **do**
    for $k \in N_z$ **do**
      if $c_{i,j,k} \in \Omega^{Band}$ **then**
        ◇ `I - Compute biased derivatives`

$$D_x^- \leftarrow \frac{\phi_{i,j,k} - \phi_{i-1,j,k}}{\Delta x_i}; \quad D_x^+ \leftarrow \frac{\phi_{i+1,j,k} - \phi_{i,j,k}}{\Delta x_i}$$
$$D_y^- \leftarrow \frac{\phi_{i,j,k} - \phi_{i,j-1,k}}{\Delta y_j}; \quad D_y^+ \leftarrow \frac{\phi_{i,j+1,k} - \phi_{i,j,k}}{\Delta y_j}$$
$$D_z^- \leftarrow \frac{\phi_{i,j,k} - \phi_{i,j,k-1}}{\Delta z_k}; \quad D_z^+ \leftarrow \frac{\phi_{i,j,k+1} - \phi_{i,j,k}}{\Delta z_k}$$

        ◇ `II - Compute biased normals`
        for $(a,b,c) \in \{-,+\}^3$ **do** ▷ `For all directions:` $\{---, --+, -+-, ...\}$
          $\mathbf{n}^{a,b,c} \leftarrow \frac{(D_x^a, D_y^b, D_z^c)}{\|(D_x^a, D_y^b, D_z^c)\| + \eta}$
          ▷ `Where` $\eta = 10^{-10}$ `is used to avoid eventual division by zero`
        end

        ◇ `III - Compare opposite biased normals to detect a kink`
        for $(a,b,c) \in \{(---),(--+),(-+-),(+--)\}$ **do** ▷ `First four directions`
          if $\|n^{a,b,c} - n^{-a,-b,-c}\|^2 > \epsilon^2$ **then** ▷ `Squaring avoids use of square root`
            $\Omega^K_{i,j,k} \leftarrow$ true ▷ `Mark` $c_{i,j,k}$ `as kink`
            cycle
          end
        end
      end
    end
  end
end
Return Ω^K

6.2. Efficient selection mask implementation

The scheme selection process is described straightforwardly in alg. 1 can be implemented in a more efficient way, from a computational point of view. The direct method consists in searching for an eventual kink in the cells part of the numerical stencil $S_d^{\pm}$ of 6 cells, leading to 6 tests for each dimension. Based on trading computational time for memory, another approach detailed in alg. 3 is derived by creating 3 (2 in 2D) supplementary arrays that will inform all cells whose numerical stencils contain at least one kink. In another way, if one cell c is known to be a kink, all surrounding cells in the x, y and z directions having a stencil $S_d^{\pm}$ containing c will be marked as unsafe.

The purpose of the algorithm is to build three Boolean arrays *mask_x*, *mask_y* and *mask_z* such as the array *mask_x* (resp. *mask_y* and *mask_z*) holds *true* if a WENO5 scheme needs to be used to compute the derivative of $\phi_{i,j,k}$ in the x-direction (resp. y and z-direction), and false otherwise, i.e. where a HOUC5 scheme can be safely used. For every cell $c_{i,j,k} \in \Omega^K$, *mask_x*, *mask_y* and *mask_z* are updated. For

$mask\_x$, all cells $\{c_{i',j,k} \mid i' \in [\![i-3, i+3]\!]\}$ are marked as *true*. A similar treatment is applied for the other directions. It can be noticed that following this strategy allows to solely use one array for each direction rather than two arrays because of upwind/downwind schemes. It may therefore include few false positives. As shown in the result section, we haven't found this to be a problem, merely because it will compute slightly more WENO5 schemes instead of HOUC5 than in the direct approach, while avoiding many redundant tests.

Algorithm 3: Pre-computation of masks for scheme selection.

```
mask_x ← false; mask_y ← false; mask_z ← false          ▷ Initialize the masks
for i ∈ N_x do
    for j ∈ N_y do
        for k ∈ N_z do
            if c_{i,j} ∈ Ω^K then                        ▷ c_{i,j,k} marked as containing a kink
                mask_x[i − 3 : i + 3, j, k] ← true
                mask_y[i, j − 3 : j + 3, k] ← true
                mask_z[i, j, k − 3 : k + 3] ← true
            end
        end
    end
end
Return [mask_x, mask_y, mask_z]
```

7. Results

7.1. Foreword

In this section, we detail the numerical framework used and propose a series of test cases to gauge the accuracy, robustness and efficiency of the proposed hybrid approach. More precisely, we will demonstrate that it is more efficient than the WENO5 scheme without compromising the accuracy.

We will first test the capability of the method from simple to complex advection test cases, involving thin layers or sharp corners. Then the coupling with the Navier-Stokes equations will be considered to assess the capability of the method to accurately and robustly capture the behavior of inviscid two-phase flows.

Alongside to this validation, we will extend the preliminary results of the section 4 concerning the anti-diffusivity on volume conservation of the HOUC5 and WENO5cons schemes on different test cases and accentuate the fact that it introduces manifest perturbations of the interface which can be disastrous over time and on its overall dynamic.

7.2. Numerical methods

7.2.1. Flow solver

The method was implemented and tested using the massively parallel open-source CFD code Notus [26], for which the following test cases are available or easily reproducible. The Navier-Stokes equations are solved on a staggered grid within a finite volume framework and a time splitting correction method for the velocity-pressure coupling [27]. A first-order semi-implicit backward difference (SBDF-1) scheme is used for the momentum equation. The inertial term is computed with a second-order Runge-Kutta integration and the associated spatial discretization scheme will be specified for each particular test case. Phase's density and viscosity are expressed as a function of the level set through a Heaviside function H_ϵ from eqs. (3) and (4), where the regularization parameter is set to $\epsilon = 2h$.

7.2.2. Level set

Advection step. As introduced previously, the temporal integration of the advection equation is done using a second-order Runge-Kutta NSSP 3,2 while the spatial discretization is done with one of the four schemes of the study: WENO5, HOUC5 or HWH5 when eq. (6) is considered, or WENO5cons for eq. (9). Moreover, since a precise value of the level set is only mandatory at the interface and its surroundings, the spatial numerical schemes of the study are only applied on a band of 12 cells from each side of the interface and a first-order upwind scheme is applied otherwise.

Reinitialization step. For all simulations, independently of the spatial scheme, the reinitialization procedure is performed since this one is essential in general case in a level set framework. The reinitialization is done by solving the H-J equation eq. (7) which is implemented based on the algorithm of [15], where the numerical parameters are fixed based on the comparative study of [6] and adapted for this work to obtain an accurate reinitialization of the level set. Hence, a second-order Runge-Kutta integration coupled with a WENO5 scheme are also used. The pseudo time step is fixed at $\Delta\tau = 0.3\Delta x$, the number of iterations for the temporal integration is set to 16 and the reinitialization procedure is done every 10 time steps.

7.3. Error measures

Several errors measurements are defined to assess the performance of the proposed method. These measures will either be computed on the whole domain Ω of cardinal N_Ω or only in the vicinity of the interface defined as Ω_{E_Γ} of cardinal N_{E_Γ}. In practice, Ω_{E_Γ} encompasses all cells inside a two-cell bandwidth centered around Γ.

Shape errors. We define the shape error, in L_2 and L_∞ norms, as the variation of ϕ from its expected value ϕ_{ex} for all cell $\mathbf{x}_l \in \Omega_{E_\Gamma}$ as:

$$E^{L_2}_{shape} = \sqrt{\frac{1}{N_{E_\Gamma}} \sum_{\mathbf{x}_l \in \Omega_{E_\Gamma}} |\phi_{ex}(\mathbf{x}_l) - \widetilde{\phi}(\mathbf{x}_l)|^2} \quad \text{and} \quad E^{L_\infty}_{shape} = \max_{\mathbf{x}_l \in \Omega_{E_\Gamma}} \left(|\phi_{ex}(\mathbf{x}_l) - \widetilde{\phi}(\mathbf{x}_l)|\right)$$

Volume conservation. The volume error E_V can be defined as:

$$E_V = \frac{|V(t) - V(t=0)|}{V(t=0)}$$

where the total volume of a phase is computed through the associated volume fractions c_i (see eq. (4)) associated to the cells of volume V_{CV_i} as: $V = \sum_i^{N_\Omega} c_i V_{\mathrm{CV}_i}$.

Error on the deviation to a signed distance function. To evaluate the quality of ϕ to be a signed distance function we used the criterion introduce in [4] which ensures that the errors is the same when the slope of ϕ is equal to α (i.e. $|\nabla\phi| = \alpha$) or to α^{-1} (i.e. $|\nabla\phi| = \alpha^{-1}$). In L_2 norm, it is given as:

$$E^{L_2}_{\nabla\phi} = \sqrt{\frac{1}{N_\Gamma} \sum_{i}^{N_\Gamma} e_{\nabla\phi}(\nabla\widetilde{\phi})^2} \quad \text{with} \quad e_{\nabla\phi}\left(\nabla\widetilde{\phi}\right) = |\ln\left(|\nabla\widetilde{\phi}|\right)|$$

The L_∞ norm of the error, noted $E^{L_\infty}_{\nabla\phi}$, is constructed similarly.

In this study, as the reinitialization step is frequent, this error measure is only considered to ensure that no severe disturbance is introduced in the level set field.

7.4. Multi-circles rotation

The first benchmark follows the idea of [4] to qualitatively overview the capacity of each method to carry and conserve small to large structures from a mesh point of view, i.e. depending on the number of cells used to represent each of them. We thus consider multiple circles of various radius, transported by rigid body rotation. As demonstrated by [28], with this particular flow, the gradient of the level set should remain unaltered and numerical errors are solely induced from the numerical resolution of the advection equation and the reinitialization procedure.

Six circles denoted as $\{C_0, C_1, C_2, C_3, C_4, C_5\}$, with respective diameter of $\{D_0, D_0 + h, D_0 + 2h, D_0 + 3h, D_0 + 4h, D_0 + 5h\}$ are uniformly initialized in a a $[0, 1]^2$ domain at a distance of 0.2 of the center. In order to study small structures, the smallest and reference diameter D_0 is set to be $3h$ large, i.e. three cells large. The mesh size is 64^2. The velocity field is constant in time and is given by:

$$(u, v) = \frac{2\pi}{T}(0.5 - y, x - 0.5) \tag{10}$$

The time step is fixed and set to $\Delta t = 1.25\text{e-}3$. The simulation is stopped after one full rotation and hence, when $t = 1$.

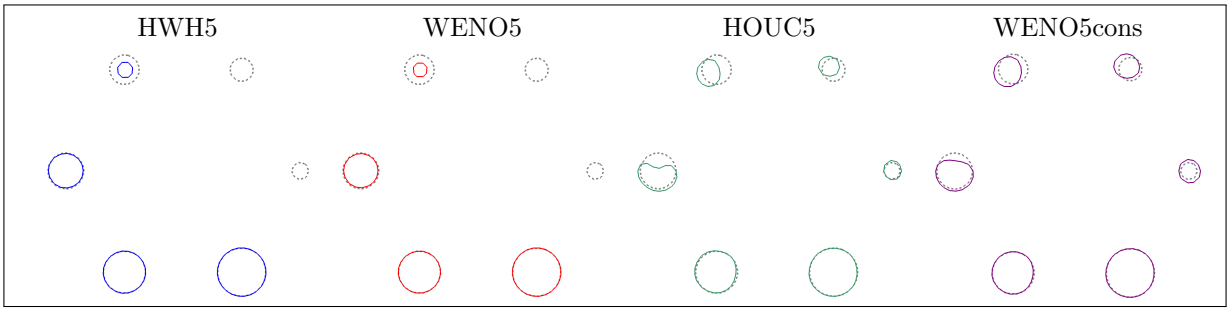

Figure 5: Interface shapes after a full rotation ($t = T = 500$) for the disk's rotation test case for a grid resolution of 64^2 cells, the reference solution is plotted in grey dashed lines. Reinitialization is performed as described in sec. 7.2.2.

As presented in figure fig. 5, after a full rotation, the proposed method HWH5 gives very similar results to the WENO5 scheme. For the smallest structures, where the interface is always close to a kink (the center point), as expected, the dissipative behaviour of these two schemes leads to a mass loss. We can see that the two smallest circles $\{C_0, C_1\}$ have vanished. However, as soon as the structure is well described by enough cells, the circles $\{C_2, C_3, C_4, C_5\}$ are well advected and conserved.

On the other hand, both HOUC5 and WENO5cons, due to their anti-diffusive behaviour, see their shape enlarged for regions close to a kink. Hence, this prevents $\{C_0, C_1\}$ to collapse. This sense of accuracy arises from the simple circular shape of these structures. However, we will see in sec. 7.6 that it is not at all desired and can lead to dreadful distortion for more complex cases. Moreover, contrary to HWH5 and WENO5 schemes, the advection of larger structures is less properly resolved. We believe that this comes from the enlargement of the level set near the kink at the center of the circle which propagates perturbations through the numerical scheme.

7.5. Single circle rotation

The purpose of this case is to validate our method on simple geometry and to study more quantitatively the proposed hybrid scheme thanks to volume and shape conservation measures as well as the deviation of the level set to a signed distance function. To do so, a mesh convergence has been performed on a single circle in rotation, using similar parameters to the previous case.

The coarsest mesh is equivalent to describing the circle with a diameter $D = 8h$ with a mesh size of $N = 64$. For this resolution, the time step is fixed and set to $\Delta t = 1.25\text{e-}3$ and it is reduced proportionally

for each finer meshes in order to keep a constant CFL number. The simulation is stopped after one full rotation and hence, when $t = 1$.

In this particular simple case, at the start, only one kink is located at the center of the circle. Thus, the proposed hybrid method will most of the time use HOUC5 and switch to WENO5 for stencils crossing cells near the center. The convergence of various error measures in fig. 6 shows that the proposed HWH5 produces equivalent results as the WENO5 scheme. This result was expected as most points in the domain stand far from kinks so that the hybrid method uses HOUC5. Comparatively, with the full WENO5 strategy, as the level set is smooth almost everywhere, smoothness indicators are very close to equality and hence the non-linear numerical scheme reduces to the optimal HOUC5 scheme. These observations induce that both strategies converge to the same result as the mesh is refined.

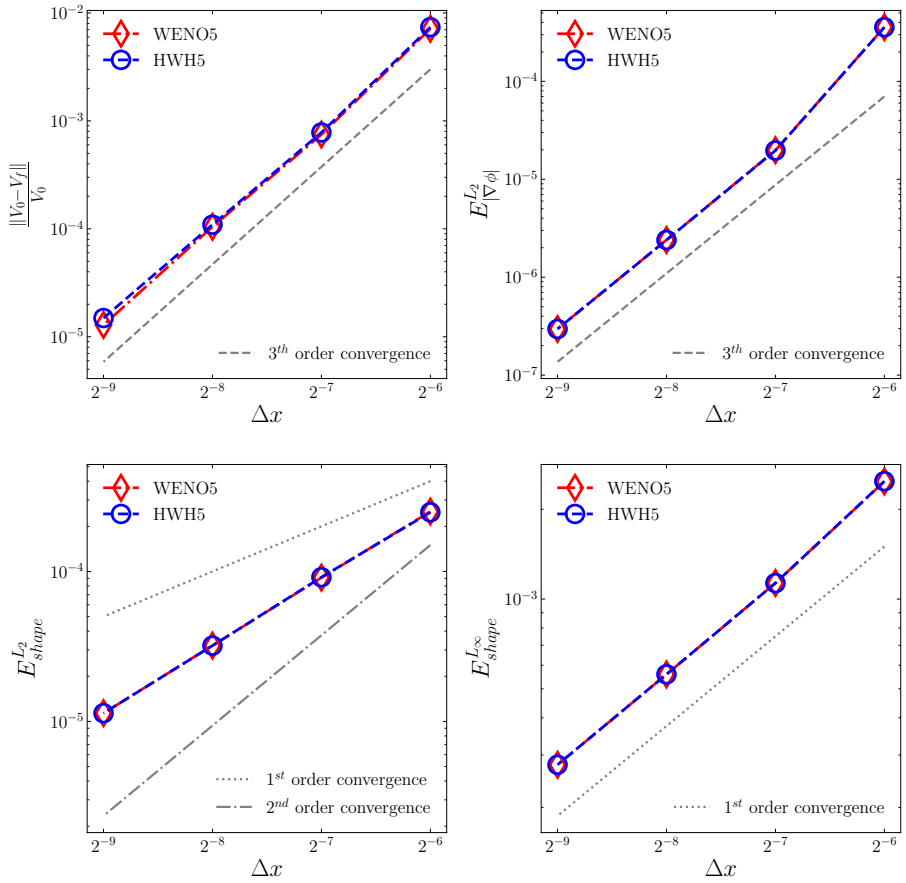

Figure 6: Single circle rotation case study. From left to right and top to bottom: convergence rate of the volume conservation, L_∞ norm for the error on the deviation to be a signed distance function ($E^{L_\infty}_{\nabla\phi}$) and the L_∞ and L_2 norm on for the shape errors ($E^{L_\infty}_{shape}$ and $E^{L_2}_{shape}$).

7.6. Single vortex 2D

We study the widely-known single vortex case [29–31] to assess the ability of the schemes to capture the interface deformation and particularly thin filaments. A $[0.0, 1.0]^2$ domain is considered, with an initial circle of a diameter $D = 0.3$ centered at (0.5, 0.75). The velocity field $(u, v) = (\frac{\partial\Psi}{\partial y}, -\frac{\partial\Psi}{\partial x})$ is derived from the stream function:

$$\Psi = \frac{1}{\pi}\sin^2(\pi x)\sin^2(\pi y)\cos(\frac{\pi t}{T}).$$

Over time, it will stretch the circle into a swirl, thinning the interface. The term $\cos(\frac{\pi t}{T})$ appearing in the velocity field definition ensures that the deformation reverses trajectories to the initial state at time T; maximal deformation is obtained at $T/2$.

First, we study all schemes' capacity to capture the evolution of the interface under large deformation. Then, a mesh convergence is performed and a comparison is done between WENO5 and the proposed HWH5 hybrid method.

7.6.1. Varying maximal deformation

As presented in the section 4, HOUC5 and WENO5cons schemes can present anti-diffusive behaviours, particularly when coupled with reinitialization, close to under-resolved regions. Here, we investigate how these schemes impact the shape of the interface when maximal deformation increases. Three different ending times $T = \{8, 12, 20\}$ for two different meshes of 128^2 and 256^2 cells are considered.

Short stretch - $T = 8$

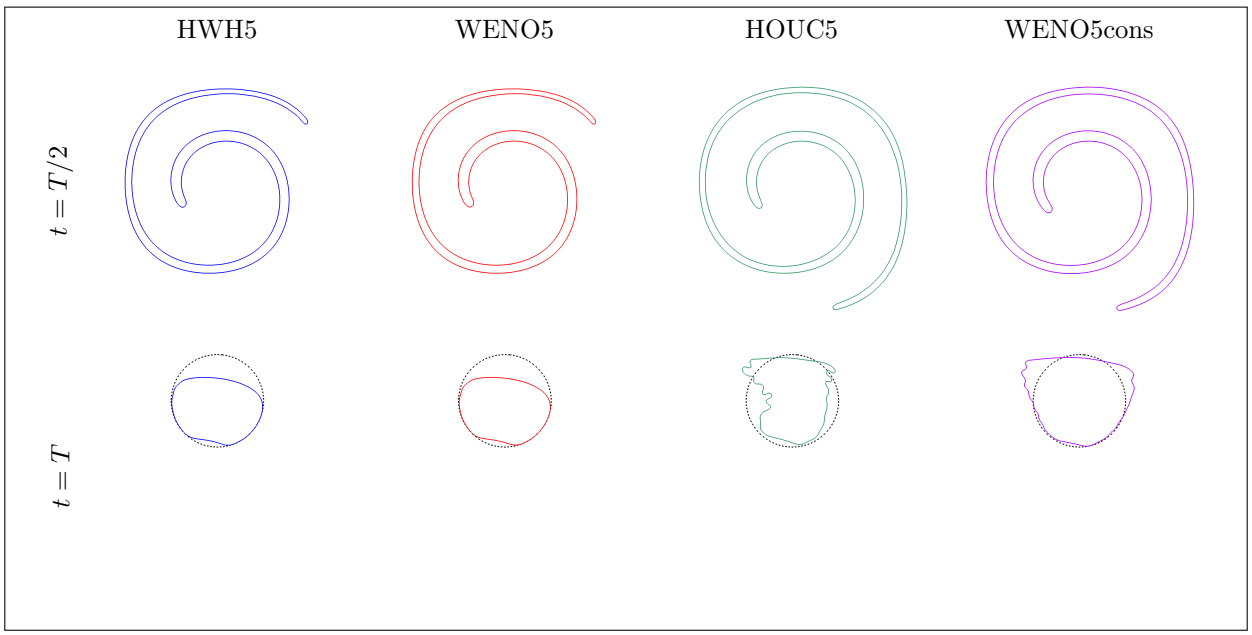

(a) 128^2 cells

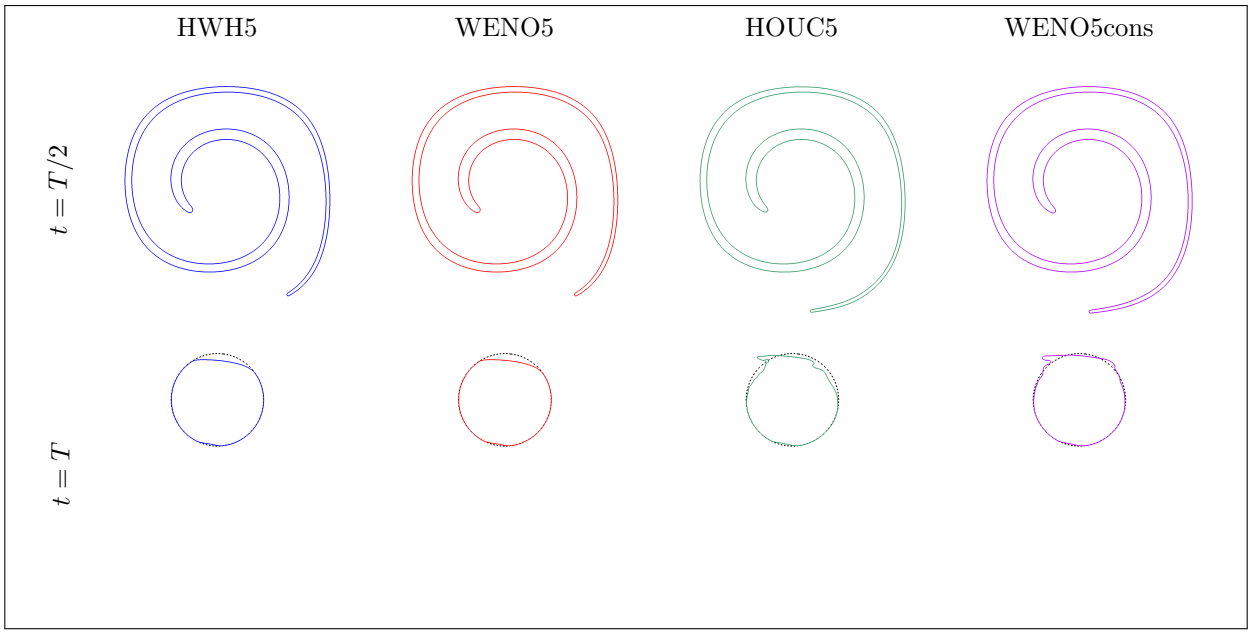

(b) 256^2 cells

Figure 7: Interface shape for the single vortex test case with $T = 8$, i.e. short stretch. For both figures, we show on top the shape at maximal deformation $t = T/2$ and, on the bottom, at $t = T$.

Intermediate stretch - $T = 12$

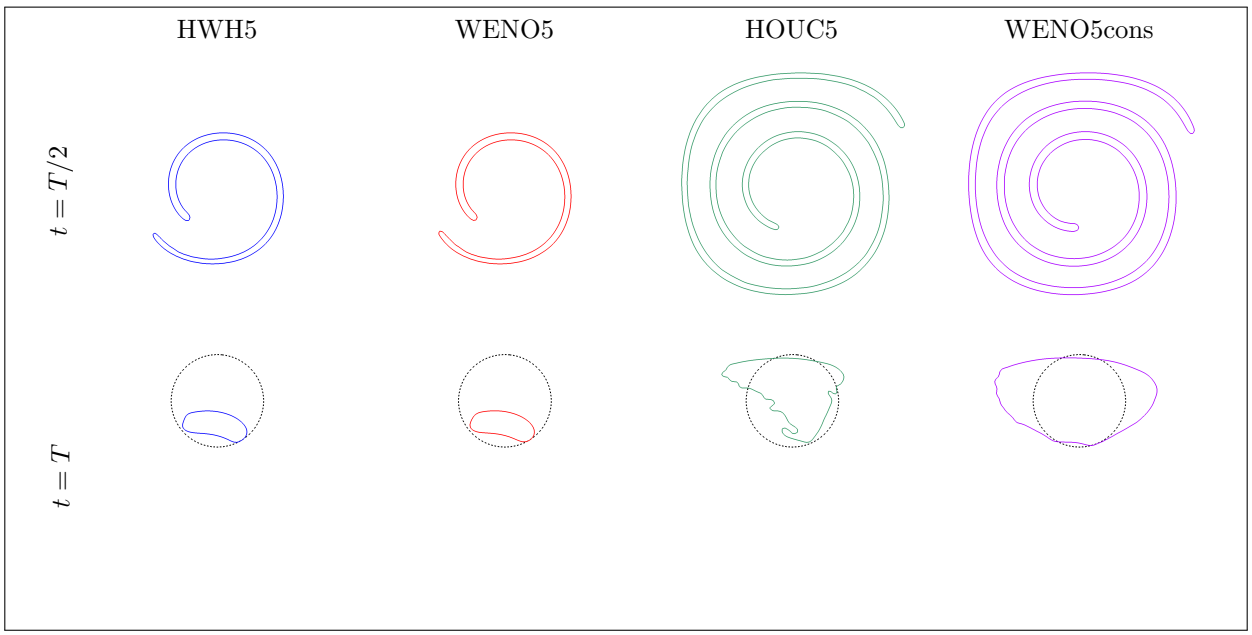

(a) 128^2 cells

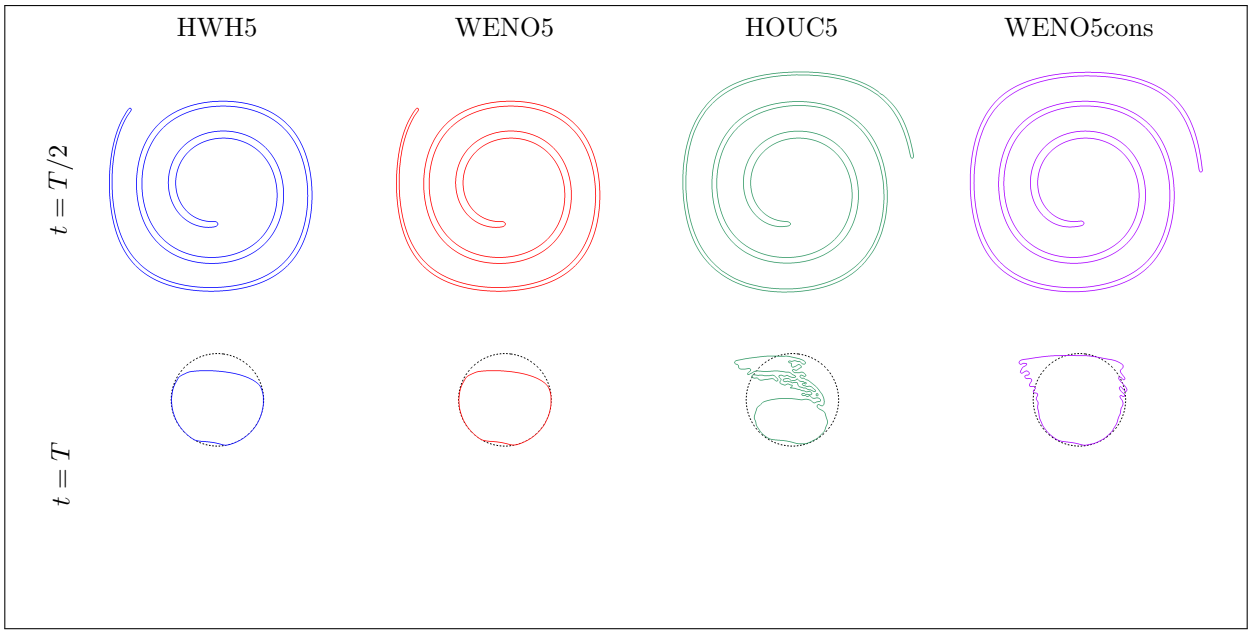

(b) 256^2 cells

Figure 8: Interface shape for the single vortex test case with $T = 12$, i.e. intermediate stretch. For both figures, we show on top the shape at maximal deformation $t = T/2$ and, on the bottom, at $t = T$.

Long stretch - $T = 20$

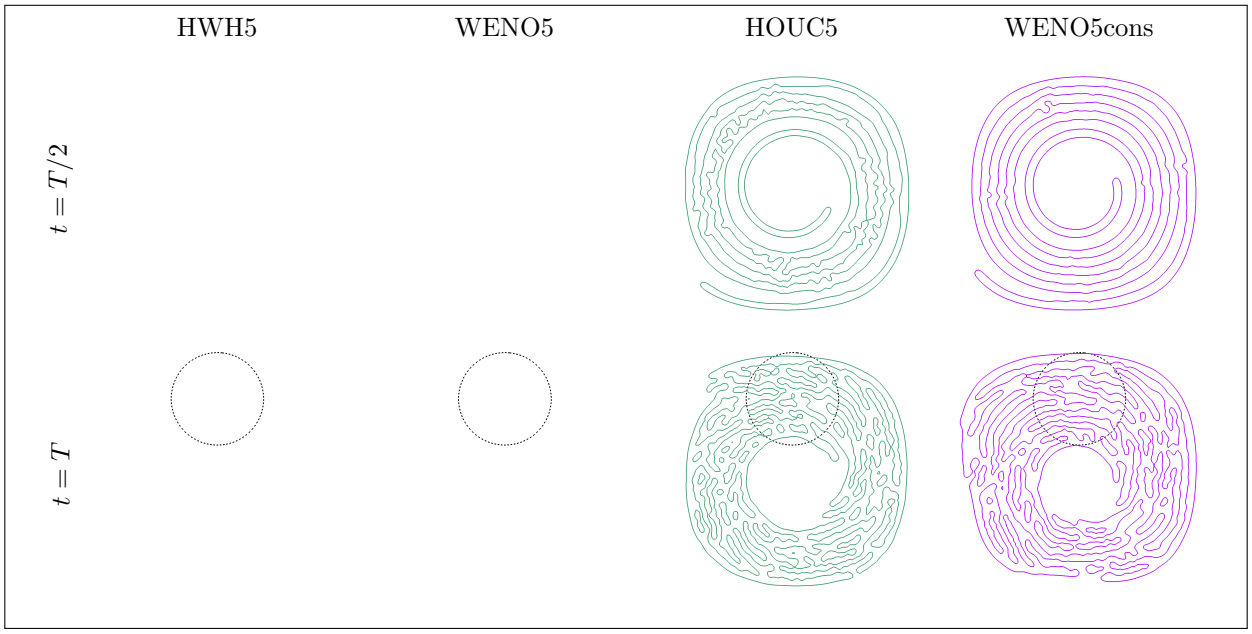

(a) 128^2 cells

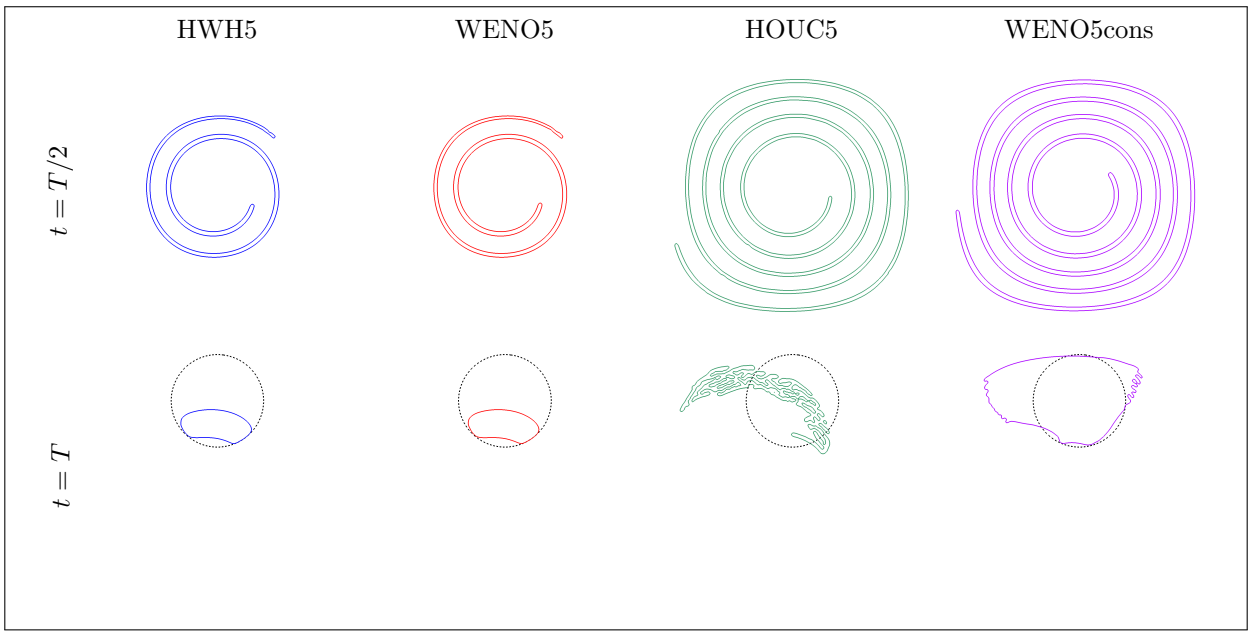

(b) 256^2 cells

Figure 9: Interface shape for the single vortex test case with $T = 20$, i.e. long stretch. For both figures, we show on top the shape at maximal deformation $t = T/2$ and, on the bottom, at $t = T$.

In figs. 7 to 9, we observe that HWH5 demonstrates very similar results to WENO5 regarding interface shape. As expected, being diffusive, both these schemes see the trailing of the interface vanish once it becomes of the order of the size of h, the grid resolution. This results in a loss of volume that clearly appears at the reversed position at $t = T$. We can note that this loss is reduced as the mesh is refined. For the longest stretch in fig. 9, at the coarsest mesh, the interface even totally vanishes because of diffusion of very thin filaments.

On the other side, both HOUC5 and WENO5cons maintain the trailing of the interface at maximal deformation for the various stretches by enlarging the thickness of that region when it becomes of the order of h. This is an interesting property as one would want to preserve thin filaments. However, for the short and intermediate stretch (fig. 7 and fig. 8), this anti-diffusive behaviour has a critical impact on the reversed shape at $t = T$. It induces perturbations that make the interface less smooth than with the HWH5 or WENO5 scheme and this anomaly is even more noticeable as the mesh is refined. For the finest mesh, HOUC5 shows its limitation as it introduces high-frequency disturbances due to the oscillatory problems of this advection scheme with non-smooth fields. Furthermore, for the longer stretching in fig. 9, we observe that both HOUC5 and WENO5cons produce ill-formed reversed shapes, particularly for the coarsest mesh. This problem is due to the over conservation of thin filaments because of anti-diffusivity. Even though the problem is reduced for the finest mesh, we see that they both induce a reversed shape that is of less quality than the smoother shape obtained with HWH5.

It is important to note that, when dealing with two-phase flows subjected to surface tension, high-frequency deformation of the interface will result in parasitic currents. Hence, smoother shapes would prevent destabilizing simulations, particularly at small scales.

7.6.2. Mesh convergence

A mesh convergence is undertaken to validate the capability of the proposed method to produce equivalent results as the WENO5 scheme on that more stressful case. We have chosen the shortest stretch ($T = 8$) which is the one usually found in the literature [2, 7]. The time step is set equal to Δt = 1.6e-3 for the coarsest grid 128^2 and is proportionally reduced as the mesh is refined. As presented in figure fig. 10, at $t = T$, regarding all errors measures (volume, signed distance function and shape error), HWH5 produces equivalent results to those of the WENO5 scheme.

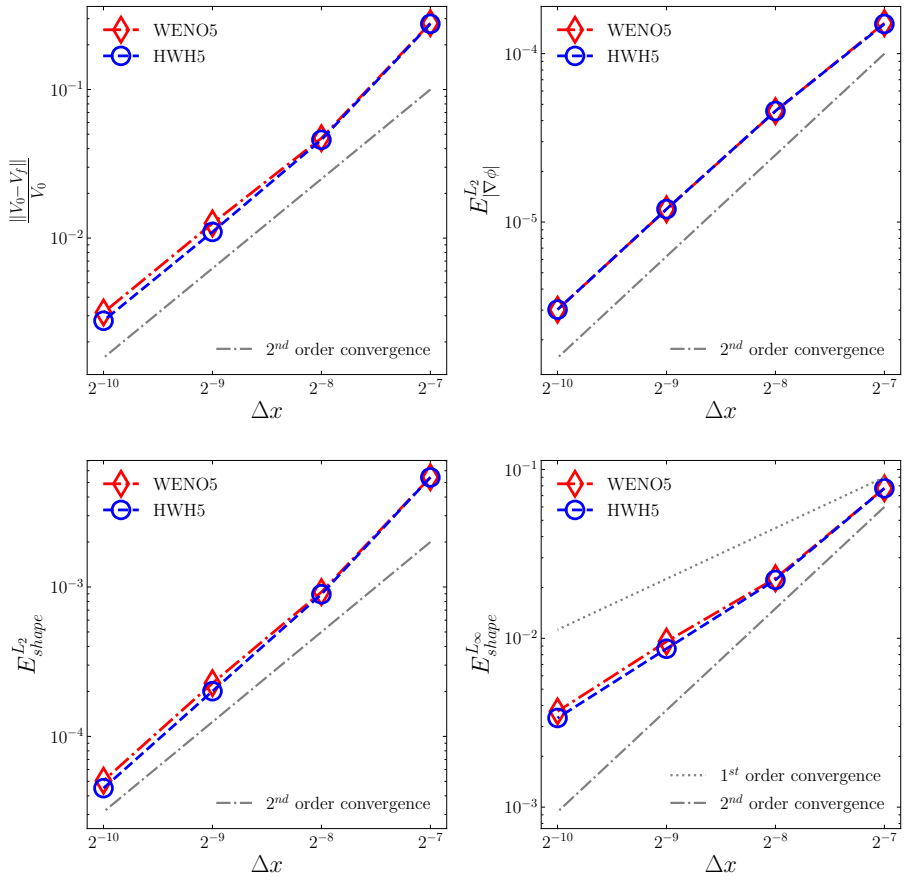

Figure 10: Single vortex 2D test case at $t = T = 8$. From left to right and top to bottom, convergence rate of volume conservation, L_∞ norm for the error on the deviation to be a signed distance function ($E^{L_\infty}_{\nabla\phi}$) and the L_∞ and L_2 norm on for the shape errors ($E^{L_\infty}_{shape}$ and $E^{L_2}_{shape}$).

7.7. Single vortex 3D

A 3D adaptation of the previous case was proposed by LeVeque [30] and applied by Enright et al. [31] to test the ability of level set methods to capture thin surfaces with deformation in both $x - y$ and $x - z$ planes. The configuration is very similar to the one in the previous section, in 3D: a $[0, 1]^3$ domain is considered where a sphere of diameter $D = 0.3$ is initialized at $(0.35, 0.35, 0.35)$. The velocity field is given by:

$$
\begin{aligned}
u =& 2\sin^2(\pi x)\sin(\pi y)\sin(\pi z)\cos(\frac{\pi t}{T}) \\
v =& 2\sin(\pi x)\sin^2(\pi y)\sin(\pi z)\cos(\frac{\pi t}{T}) \\
z =& 2\sin(\pi x)\sin(\pi y)\sin^2(\pi z)\cos(\frac{\pi t}{T}).
\end{aligned}
$$

where the same term $\cos(\frac{\pi t}{T})$ ensures that the interface will go back to its initial state at $t = T$ and that maximal deformation is obtained at $t = T/2$. Here, we have used $T = 3$. Table 1 shows that HWH5 is also robust in 3D and gives, as desired, equivalent results to the ones obtained with WENO5.

	$\lvert\frac{V_0-V_{final}}{V_0}\rvert$		$E^{L_\infty}_{\nabla\phi}$		$E^{L_2}_{shape}$		$E^{L_\infty}_{shape}$	
Method	128^2	256^2	128^2	256^2	128^2	256^2	128^2	256^2
WENO5	1.41e-01	1.00e-02	2.24e-02	1.34e-03	3.49e-03	1.49e-04	1.56e-01	1.73e-02
HWH5	1.32e-01	9.66e-03	2.10e-02	1.00e-03	3.43e-03	1.60e-04	1.56e-01	2.27e-02

Table 1: Numerical results of the single vortex 3D case at $t = T = 3$ on the enclosed volume error, the L_∞ norm on the deviation to be a signed distance function $E^{L_\infty}_{\nabla\phi}$, the L_2 norm on the shape error ($E^{L_2}_{shape}$) and L_∞ norm on the shape error ($E^{L_\infty}_{shape}$).

7.8. Zalesak disk

This test case follows the one proposed in [32] to appraise the capacity of the reinitialization method to preserve sharp corners on the interface. In our case, it is also an interesting test as the Zalesak disk induces inherent kinks in the slot and inside the shape, as illustrated later in fig. 14a. It is thus a stressing configuration for our hybrid approach.

In a $[0, 1]^2$ domain, a slotted disk is initially centered at $(0.5, 0.75)$ with a diameter of $D = 0.3$ and a slot of 0.05 of width and 0.25 of length. The velocity field is set to transport the interface in a counterclockwise rotation around the point $(0.5, 0.5)$ and is defined as:

$$(u, v) = (0.5 - y, x - 0.5) \tag{11}$$

As in the literature, the time step is fixed to $\Delta t = 2\pi/628$ for the corresponding mesh of 100^2 cells, and it is adapted proportionally for other meshes. The simulation is stopped after one full rotation of the slotted disk which corresponds at a time $t = 2\pi$. In this test case, as in the previous ones, numerical errors principally originate from the advection schemes and the reinitialization. As illustrated in fig. 11, the HWH5 scheme shows almost identical results to the WENO5 scheme on the interface shape, even in presence of kinks located on the interface near the two sharp corners.

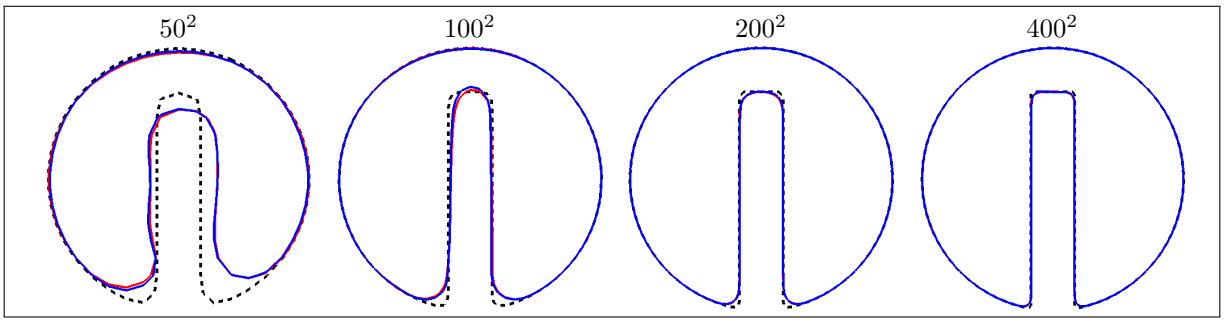

Figure 11: Interface shape after one rotation for the Zalesak disk case. Results with WENO5 are presented in red, HWH5 in blue and the dashed line represents the initial interface.

7.9. 2D column at equilibrium - spurious currents at fixed Laplace number

We propose to validate that the proposed method does not introduce spurious numerical oscillations in high-order derivatives of ϕ and allows accurate computation of curvature. It should thus capture correctly surface tension forces, which are dominant at small scales, and, for that purpose, we study the parasitic currents arising from discretization errors, as evaluated in [33–35].

A 2D column at rest is considered, with a diameter $D = 0.4$ at the center of $[0, 1]^2$ square. Both density and viscosity are constant for all simulations and equal to 1 in each phase. In order to study the spatial convergence of parasitic currents, the Laplace number ($La = \sigma\rho L/\mu^2$) is fixed at 120 for a mesh resolution varying from 32^2 to 256^2 cells. No-slip conditions are applied to all boundaries. The time step is kept

constant, Δt = 3e-6, for all meshes, thus respecting the constraint given by the revised capillary time step constraint [34] for the finest mesh. Simulations have been conducted until a numerical steady state has been attained, i.e. when spurious currents appear to have reached a minimum.

A scaled maximum capillary number $\mathrm{Ca}_{max} = \mathrm{Ca}^*_{max}/U_\sigma$ is considered for the results, where the characteristic velocity is defined as $U_\sigma = \sqrt{\sigma/(\rho D)}$ and the usual capillary number as $\mathrm{Ca}^*_{max} = \mu|\mathbf{u}|_{max}/\sigma$. Also, time is adimenzionalized as $t_\sigma = t/T_\sigma$, with $T_\sigma = \sqrt{\rho D^3/\sigma}$.

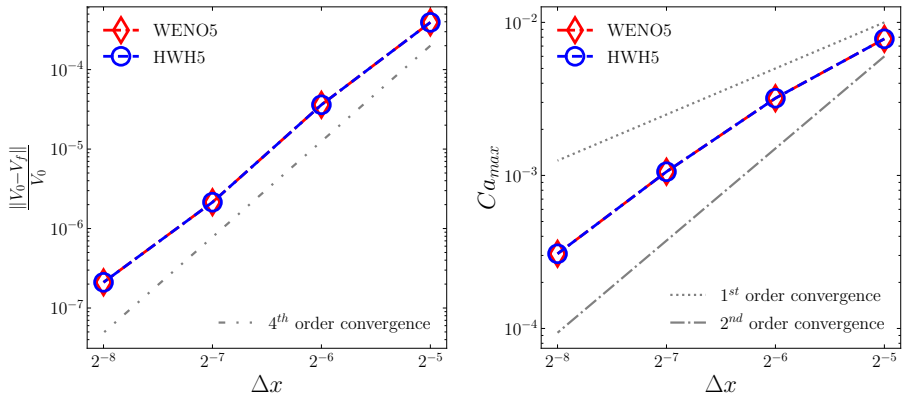

Figure 12: Convergence study of the 2D column at equilibrium for the enclosed volume variation (left) and Ca_{max} (right) at $La = 120$ for WENO5 and HWH5, when a steady state has been reached.

Figure fig. 12 shows that HWH5 produces very equivalent results as WENO5 on the convergence of the scaled maximum capillary number and as well as for errors on the enclosed volume. This result was expected as the only kink present in this test case is at the center of the circle and far away from the interface for the different mesh resolutions. Moreover, even with the presence of parasitic currents, the variation of the level set between two iterations is moderate. Hence, when the WENO5 scheme is computed, all the non-linear weights will be the same at the interface and its vicinity and consequently, this will be the same as using a HOUC5 scheme.

7.10. Rayleigh-Taylor instability

The last test case presented in this study is the Rayleigh-Taylor instability case without surface tension. The main purpose is to demonstrate the performance of the proposed method in a more complex flow, more stressful for the level set field, and where numerous thin filaments, i.e. under-resolved structures, topology changes and hence kinks appear. Herein, we follow the set up as in [6, 36–38]. In a domain of size $[d, 4d]$, we initially define the interface as $\phi_0(x, y) = y - d(2 + 0.1\cos(2\pi x/d))$. Gravity is taken into account and the gravitational acceleration is denoted by g. Surface tension is not considered in this test case since it is not necessary to obtain the desired results (thin filaments, under-resolved structures and topology changes) and would make the simulation more demanding.

Boundary conditions are periodic in the x-direction and no-slip in the other direction. The heaviest (resp. lightest) fluid has density ρ_h (resp. ρ_l) and viscosity μ is the same for both fluids. The dynamic of the flow is characterised by the Atwood number $A = (\rho_h - \rho_l)/(\rho_h + \rho_l)$ and the Reynolds number $Re = \rho_h d\sqrt{gd}/\mu$. In our case, we chose $A = 0.5$ and $Re = 3000$.

As presented in fig. 13, the HWH5 scheme produces very similar results compared to WENO5. Hence, this last test case validates that the hybrid method has comparable accuracy and robustness to the sole WENO5 scheme, even for a complex flow with small structures. For an illustration of the kink map on that test case, the reader can refer to fig. 14.

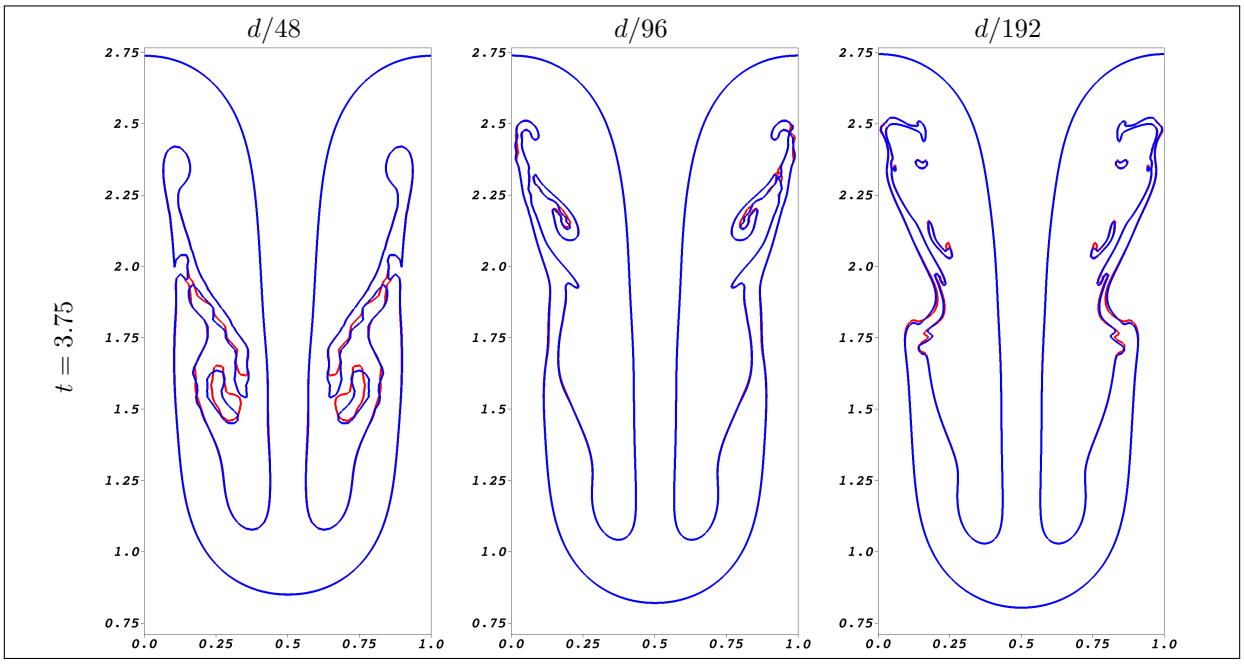

Figure 13: Interface shape at $t = 3.75$ for the Rayleigh-Taylor instability test case. The WENO5 method is represented in red, the HWH5 method in blue.

7.11. Computational time

The principal purpose of the proposed hybrid method is to obtain a scheme that has equivalent accuracy to WENO5 with a reduced computational cost. This section is devoted to investigating the numerical cost of the hybrid method comparatively to the use of a sole WENO5 method.

Herein, we have measured the total cost of the advection procedure for comparison. For WENO5, solely the cost for computing the $\mathbf{u} \cdot \nabla\phi$ term is measured while, for HWH5, we also counted the supplementary detection of kinks and scheme selection process. The results are processed in order to obtain the speedup factor of the HWH5 such as:

$$\text{Speedup factor} = \frac{\text{CPU time for WENO5}}{\text{CPU time for HWH5}}$$

The overall gain obtained by the proposed algorithm, as reported in tables 2 and 3, climbs up to 2, leading to a 50% CPU cost reduction in the most favorable cases. Also, in order to provide a finer analysis, we tracked τ, the average relative number of HOUC5 calls against the total number of derivative computation, namely:

$$\tau = \frac{N_{\text{HOUC5}}}{N_{\text{HOUC5}} + N_{\text{WENO5}}} = \frac{N_{\text{HOUC5}}}{N_{\text{HWH5}}}. \tag{12}$$

Moreover, the HWH5 overhead cost of computing the kink map and the hybrid masks is reported as its ratio over the overall cost:

$$\beta = \frac{\text{CPU time for overhead}}{\text{CPU time for HWH5}}. \tag{13}$$

In practice, of course, more overhead adds up, coming from 3D arrays memory access, processor cache exchange, etc. that we will refer as computation overhead. Moreover, we have excluded the supplementary costs of parallel exchanges in the CPU time measures because they are independent on the proposed method and are particularly sensitive to implementation and hardware matters.

Nevertheless, in order to supply a good estimate of the maximum expected gain, we first measured the

average computational cost of the sole HOUC5 and WENO5 schemes by evaluating the functions millions of times on fictitious data. The optimized version of the WENO5 scheme, as detailed in appendix A, shows a unit speedup around 4 in favor of the HOUC5 scheme, as expected by the fewer number of numerical operations needed. We also have tested the solving of the 3D advection equation on practical cases of level set advection and, due to the computation overheads as discussed above, the maximum effective speedup is between 2 and 3.

	Resolution	Speedup factor	τ (%)	β (%)
Zalesak disk	50^2	1.2	76	5
	100^2	1.4	81	5
	200^2	1.7	85	7
	400^2	1.8	92	7
Advection one circle	32^2	1.3	96	11
	64^2	1.5	98	7
	128^2	1.9	99	11
	256^2	1.7	99	10
	512^2	1.3	100	8
Single vortex 2D	128^2	1.5	81	7
	256^2	2.0	88	7
	512^2	1.7	90	8
	1024^2	1.4	95	10
Single vortex 3D	128^3	1.4	92	11
	256^3	1.4	94	8
Rayleigh-Taylor	$d/48$	1.3	74	8
	$d/96$	1.5	82	7
	$d/192$	1.6	90	7

Table 2: Speedup factor for the hybrid HWH5 method compared to WENO5 for different test cases with various mesh resolutions, using 16 parallel threads. Also indicating τ, the portion of HOUC5 in the hybrid scheme (see eq. (12)) and β the portion of computational time of the overhead (see eq. (13)).

For the different test cases studied above, we have measured the CPU usage for the hybrid HWH5 method as well as for WENO5. As computing the solutions for the finest mesh using only 1 thread wouldn't be righteous nor representative of practical applications, we have chosen to compare 16 and 32 parallel threads results for all simulations, on various meshes, in order to obtain a wider overview of computational costs. While a full scalability analysis is out of the scope of this article, we have found these partitions to be representative and cover most practical cases, and the results well according. Calculations were carried out on the CURTA cluster of MCIA (Mesocentre for Intensive Calculation in the Aquitaine French region) on one node of 32 cores on 2 sockets of an Intel ®Xeon ®Gold SKL-6130 2,1 GHz.

We have reported in table 2 (16 threads) and table 3 (32 threads), the measures for all simulations: the proposed hybrid method shows an overall speedup factor up to 2.1 for 2D cases. For the 3D case, as the number of cells per thread is largely increased, even with a fair proportion of HOUC5 ($\tau \geq 92\%$), the overall speedup factor is around 1.4 which is still substantial, particularly in 3D. The reader may observer an optimal number of cells per thread that maximizes the gain for every simulation. For 16 or 32 threads, it corresponds to meshes between 256^2 and 512^2. Below or above, computation overheads play a more important role that reduces the overall gain.

It is worthy to note that, in some particular cases where the interface shape is bound to have relatively many kinks, HWH5 may have an overall cost higher than the use of a WENO5 scheme because most points will be computed with the more expensive WENO5 scheme added to the overhead cost for detecting kinks. This would be particularly the case when the interface is made of numerous small structures, relative to cells

	Resolution	Speedup factor	τ (%)	β (%)
Zalesak disk	50^2	-	-	-
	100^2	1.2	81	7
	200^2	1.5	85	8
	400^2	1.8	92	9

	Resolution	Speedup factor	τ (%)	β (%)
Advection one circle	32^2	-	-	-
	64^2	1.5	98	9
	128^2	2.0	99	11
	256^2	2.0	99	12
	512^2	1.7	100	11

	Resolution	Speedup factor	τ (%)	β (%)
Single vortex 2D	128^2	1.4	81	11
	256^2	2.0	88	9
	512^2	2.1	90	6
	1024^2	1.8	95	9

	Resolution	Speedup factor	τ (%)	β (%)
Single vortex 3D	128^3	1.5	92	11
	256^3	1.4	94	10

	Resolution	Speedup factor	τ (%)	β (%)
Rayleigh-Taylor	$d/48$	1.3	74	10
	$d/96$	1.5	82	8
	$d/192$	1.6	90	7

Table 3: Speedup factor for the hybrid HWH5 method compared to WENO5 for different test cases with various mesh resolutions, using 32 parallel threads. Also indicating τ, the portion of HOUC5 in the hybrid scheme (see eq. (12)) and β the portion of computational time of the overhead (see eq. (13)). Two low resolutions have not been computed here because of the too small (< 80) proportion of cells per thread.

size. It should be stressed that the CPU cost is also linked to the number of points surrounding the surface relatively to the total number of points in the computational domain. Indeed, computational overheads as well as β can represent a larger portion of the costs for the same τ, as observed in the results.

Moreover, since inherent kinks are points present on the medial axis of the level set or because of a numerical discrepancy, as presented for example on fig. 14a, the finer the mesh, the lower the portion of those cells compared to the total number of cells. The measure of the portion τ of the HOUC5 scheme in tables 2 and 3 shows that for finer mesh, with relatively less kinks, HOUC5 scheme is favored and thus the overall computational time decreases. In these cases, the speedup increases up significantly to 2.

8. Conclusion

We have presented a robust, accurate and efficient hybrid strategy, HWH5, coupling WENO5 and HOUC5 schemes, which preserves the robustness of the former in regions where the spatial discretization of the advection equation is subject to large errors, and also benefits from the efficiency of the latter for all other *safe* regions. An efficient implementation of kink detection permits reducing the overhead computational effort. The capacity of this approach is demonstrated in a variety of benchmarks, where the hybrid method presents equivalent results as the WENO5 scheme for a computational cost lowered down to 50%.

We have also presented that the sole use of the HOUC5 scheme or the WENO5cons method for solving the advection equation presents anti-diffusive behaviors on the volume conservation and may lead to introducing noticeable perturbations of the interface which can be dreadful over time, particularly regarding two-phase flows. While the introduced scheme, with an adequate coupling thanks to the kink map, presents diffusive results, allowing to obtain a method as robust as the WENO5 scheme for a reduced computational.

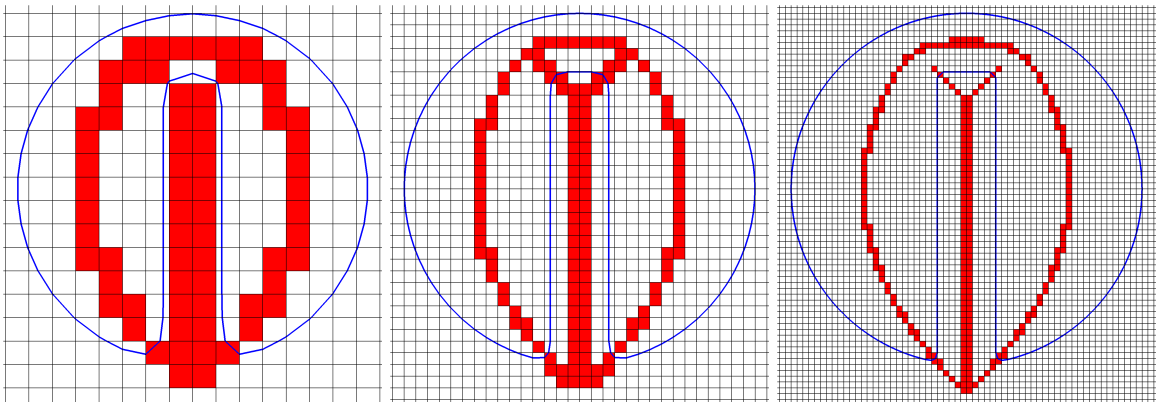

(a) Zalesak test case (see sec. 7.8): initial shape for a grid resolution of 64^2 (left), 128^2 (center) and 256^2 (right) cells.

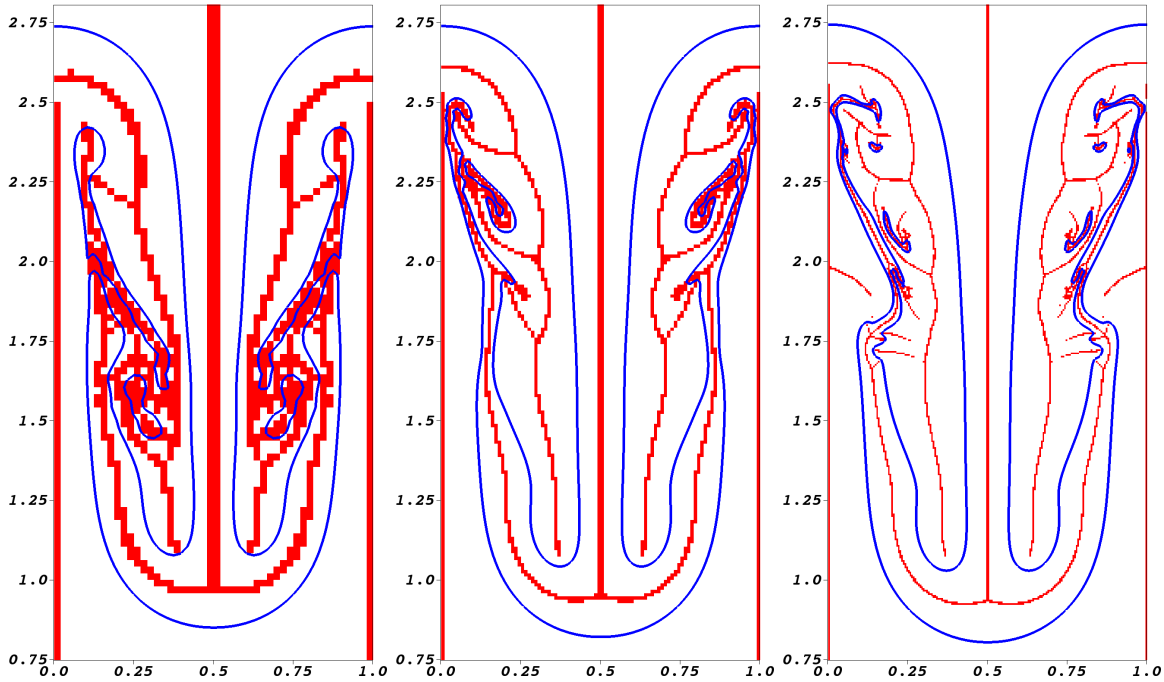

(b) Rayleigh-Taylor test case (see sec. 7.10, at $t = 3.75$ for a grid resolution of $d/48$ (left), $d/96$ (center) and $d/192$ (right) cells. Here, for illustration purpose, the kink detection algorithm was applied on the whole domain, farther than practically needed by the level set band.

Figure 14: Illustration of the kink detection algorithm of [4] on two cases. For all figures, the interface is drawn in blue and the detected kink cells are marked in red. The underlying grid is shown in grey. As illustrated in both test cases, the portion of kinks comparatively to the number of cells decreases when refining the mesh since inherent kinks are solely part of the medial axis of the level set. Thus, the HOUC5 scheme will be favored instead of WENO5.

A. Efficient implementation of the WENO5 scheme

In order to minimize the CPU cost for evaluating WENO5 and to obtain the fairest comparison with HOUC5, we present below an efficient implementation of the scheme in its Z version, as used in the code.

Algorithm 4: Efficient implementation of the WENO5-Z upwind scheme. The discrete field is given as input through the array $\psi_{-3} \to \psi_{+2}$, the spatial step is Δ.

$\epsilon \leftarrow 10^{-6}$; $C_{13/3} \leftarrow 13/3$ ▷ `Pre-computed constants`

for $l \in [-2, +2]$ **do** ▷ `First order derivatives`
  $v_l \leftarrow (\psi_l - \psi_{l-1})/\Delta$
end

▷ `Smoothness indicators`
$IS_1 \leftarrow C_{13/3}\,(v_1 - 2v_2 + v_3)^2 + (v_1 - 4v_2 + 3v_3)^2$
$IS_2 \leftarrow C_{13/3}\,(v_2 - 2v_3 + v_4)^2 + (v_2 - v_4)^2$
$IS_3 \leftarrow C_{13/3}\,(v_3 - 2v_4 + v_5)^2 + (3v_3 - 4v_4 + v_5)^2$

▷ `WENO5-Z weights`
$\gamma \leftarrow |IS_1 - IS_3|$
$a_1 \leftarrow (1 + \gamma/(\epsilon + IS_1))^2$
$a_2 \leftarrow 6\,(1 + \gamma/(\epsilon + IS_2))^2$
$a_3 \leftarrow 3\,(1 + \gamma/(\epsilon + IS_3))^2$

result $\leftarrow a_1\,(2v_1 - 7v_2 + 11v_3)$
result $\leftarrow$ result $+ a_2\,(-v_2 + 5v_3 + 2v_4)$
result $\leftarrow$ result $+ a_3\,(2v_3 + 5v_4 - v_5)$
result $\leftarrow$ result $\times\, 10/(a_1 + a_2 + a_3)$ ▷ `Weights normalization`

Return result

References

[1] S. Osher, J. A. Sethian, Fronts propagating with curvature-dependent speed: Algorithms based on Hamilton-Jacobi formulations, Journal of Computational Physics 79 (1) (1988) 12–49. doi:10.1016/0021-9991(88)90002-2.
URL http://www.sciencedirect.com/science/article/pii/0021999188900022

[2] D. Hartmann, M. Meinke, W. Schröder, The constrained reinitialization equation for level set methods, Journal of Computational Physics 229 (5) (2010) 1514–1535. doi:10.1016/j.jcp.2009.10.042.
URL https://linkinghub.elsevier.com/retrieve/pii/S0021999109006032

[3] G. Russo, P. Smereka, A Remark on Computing Distance Functions, Journal of Computational Physics 163 (1) (2000) 51–67. doi:10.1006/jcph.2000.6553.
URL http://www.sciencedirect.com/science/article/pii/S0021999100965537

[4] F. Henri, M. Coquerelle, P. Lubin, Geometric level set reinitialization using closest points method, Submitted to Journal of Computational Physics - Under revision (2021).

[5] K. Luo, C. Shao, Y. Yang, J. Fan, A mass conserving level set method for detailed numerical simulation of liquid atomization, Journal of Computational Physics 298 (2015) 495–519. doi:10.1016/j.jcp.2015.06.009.
URL https://www.sciencedirect.com/science/article/pii/S0021999115003952

[6] Z. Solomenko, P. D. M. Spelt, L. Ó Náraigh, P. Alix, Mass conservation and reduction of parasitic interfacial waves in level-set methods for the numerical simulation of two-phase flows: A comparative study, International Journal of Multiphase Flow 95 (2017) 235–256. doi:10.1016/j.ijmultiphaseflow.2017.06.004.
URL http://www.sciencedirect.com/science/article/pii/S0301932216304669

[7] R. R. Nourgaliev, T. G. Theofanous, High-fidelity interface tracking in compressible flows: Unlimited anchored adaptive level set, Journal of Computational Physics 224 (2) (2007) 836–866. doi:10.1016/j.jcp.2006.10.031.
URL https://www.sciencedirect.com/science/article/pii/S0021999106005511

[8] G.-S. Jiang, C.-W. Shu, Efficient Implementation of Weighted ENO Schemes, Journal of Computational Physics 126 (1) (1996) 202–228. doi:10.1006/jcph.1996.0130.
URL http://www.sciencedirect.com/science/article/pii/S0021999196901308

[9] F. Couderc, Développement d'un code de calcul pour la simulation d'écoulements de fluides non miscibles. Application à la désintégration assistée d'un jet liquide par un courant gazeux., phdthesis, Ecole nationale superieure de l'aeronautique et de l'espace (Feb. 2007).
URL https://tel.archives-ouvertes.fr/tel-00143709

[10] S. Tanguy, Développement d'une méthode de suivi d'interface. Applications aux écoulements diphasiques, These de doctorat, Rouen (Jan. 2004).
URL https://www.theses.fr/2004ROUES059
[11] K. Voronetska, Simulation numérique directe des écoulements à phases dispersées, These de doctorat, Bordeaux 1 (Mar. 2012).
URL http://www.theses.fr/2012BOR14507
[12] T. Abadie, J. Aubin, D. Legendre, On the combined effects of surface tension force calculation and interface advection on spurious currents within volume of fluid and level set frameworks, Journal of Computational Physics 297 (2015) 611–636. doi:10.1016/j.jcp.2015.04.054.
URL https://linkinghub.elsevier.com/retrieve/pii/S0021999115003113
[13] I. Kataoka, Local instant formulation of two-phase flow, International Journal of Multiphase Flow 12 (5) (1986) 745–758. doi:10.1016/0301-9322(86)90049-2.
URL http://www.sciencedirect.com/science/article/pii/0301932286900492
[14] J. U. Brackbill, D. B. Kothe, C. Zemach, A continuum method for modeling surface tension, Journal of Computational Physics 100 (2) (1992) 335–354. doi:10.1016/0021-9991(92)90240-Y.
URL http://www.sciencedirect.com/science/article/pii/002199919290240Y
[15] M. Sussman, P. Smereka, S. Osher, A Level Set Approach for Computing Solutions to Incompressible Two-Phase Flow, Journal of Computational Physics 114 (1) (1994) 146–159. doi:10.1006/jcph.1994.1155.
URL http://www.sciencedirect.com/science/article/pii/S0021999184711557
[16] M. Sussman, E. Fatemi, An Efficient, Interface-Preserving Level Set Redistancing Algorithm and Its Application to Interfacial Incompressible Fluid Flow, SIAM Journal on Scientific Computing 20 (4) (1999) 1165–1191, publisher: Society for Industrial and Applied Mathematics. doi:10.1137/S1064827596298245.
URL https://epubs.siam.org/doi/abs/10.1137/S1064827596298245
[17] J. C. Butcher, Numerical methods for ordinary di erential equations in the 20th century, Journal of Computational and Applied Mathematics (2000) 29.
[18] C.-W. Shu, S. Osher, Efficient implementation of essentially non-oscillatory shock-capturing schemes, Journal of Computational Physics 77 (2) (1988) 439–471. doi:10.1016/0021-9991(88)90177-5.
URL https://linkinghub.elsevier.com/retrieve/pii/0021999188901775
[19] A. K. Henrick, T. D. Aslam, J. M. Powers, Mapped weighted essentially non-oscillatory schemes: Achieving optimal order near critical points, Journal of Computational Physics 207 (2) (2005) 542–567. doi:10.1016/j.jcp.2005.01.023.
URL https://www.sciencedirect.com/science/article/pii/S0021999105000409
[20] R. Borges, M. Carmona, B. Costa, W. S. Don, An improved weighted essentially non-oscillatory scheme for hyperbolic conservation laws, Journal of Computational Physics 227 (6) (2008) 3191–3211. doi:10.1016/j.jcp.2007.11.038.
URL https://www.sciencedirect.com/science/article/pii/S0021999107005232
[21] M. Castro, B. Costa, W. S. Don, High order weighted essentially non-oscillatory WENO-Z schemes for hyperbolic conservation laws, Journal of Computational Physics 230 (5) (2011) 1766–1792. doi:10.1016/j.jcp.2010.11.028.
URL https://www.sciencedirect.com/science/article/pii/S0021999110006431
[22] E. Olsson, G. Kreiss, A conservative level set method for two phase flow, Journal of Computational Physics 210 (1) (2005) 225–246. doi:10.1016/j.jcp.2005.04.007.
URL https://www.sciencedirect.com/science/article/pii/S0021999105002184
[23] E. Olsson, G. Kreiss, S. Zahedi, A conservative level set method for two phase flow II, Journal of Computational Physics 225 (1) (2007) 785–807. doi:10.1016/j.jcp.2006.12.027.
URL https://www.sciencedirect.com/science/article/pii/S0021999107000046
[24] P. Macklin, J. Lowengrub, Evolving interfaces via gradients of geometry-dependent interior Poisson problems: application to tumor growth, Journal of Computational Physics 203 (1) (2005) 191–220. doi:10.1016/j.jcp.2004.08.010.
URL https://www.sciencedirect.com/science/article/pii/S0021999104003249
[25] A. Ervik, K. Y. Lervag, S. T. Munkejord, A robust method for calculating interface curvature and normal vectors using an extracted local level set, Journal of Computational Physics 257 (2014) 259–277. doi:10.1016/j.jcp.2013.09.053.
URL http://www.sciencedirect.com/science/article/pii/S0021999113006712
[26] Notus – Computational Fluid Dynamics.
URL https://notus-cfd.org/
[27] K. Goda, A multistep technique with implicit difference schemes for calculating two- or three-dimensional cavity flows, Journal of Computational Physics 30 (1) (1979) 76–95. doi:10.1016/0021-9991(79)90088-3.
URL http://www.sciencedirect.com/science/article/pii/0021999179900883
[28] M. F. Trujillo, L. Anumolu, D. Ryddner, The distortion of the level set gradient under advection, Journal of Computational Physics 334 (2017) 81–101. doi:10.1016/j.jcp.2016.11.050.
URL http://www.sciencedirect.com/science/article/pii/S0021999116307045
[29] J. B. Bell, P. Colella, H. M. Glaz, A second-order projection method for the incompressible navier-stokes equations, Journal of Computational Physics 85 (2) (1989) 257–283. doi:10.1016/0021-9991(89)90151-4.
URL http://www.sciencedirect.com/science/article/pii/0021999189901514
[30] R. J. LeVeque, High-Resolution Conservative Algorithms for Advection in Incompressible Flow, SIAM Journal on Numerical Analysis 33 (2) (1996) 627–665, publisher: Society for Industrial and Applied Mathematics. doi:10.1137/0733033.
URL https://epubs.siam.org/doi/abs/10.1137/0733033
[31] D. Enright, R. Fedkiw, J. Ferziger, I. Mitchell, A Hybrid Particle Level Set Method for Improved Interface Capturing, Journal of Computational Physics 183 (1) (2002) 83–116. doi:10.1006/jcph.2002.7166.

URL http://www.sciencedirect.com/science/article/pii/S0021999102971664
[32] S. T. Zalesak, Fully multidimensional flux-corrected transport algorithms for fluids, Journal of Computational Physics 31 (3) (1979) 335–362. doi:10.1016/0021-9991(79)90051-2.
URL http://www.sciencedirect.com/science/article/pii/0021999179900512
[33] M. M. Francois, S. J. Cummins, E. D. Dendy, D. B. Kothe, J. M. Sicilian, M. W. Williams, A balanced-force algorithm for continuous and sharp interfacial surface tension models within a volume tracking framework, Journal of Computational Physics 213 (1) (2006) 141–173. doi:10.1016/j.jcp.2005.08.004.
URL http://www.sciencedirect.com/science/article/pii/S0021999105003748
[34] F. Denner, B. G. M. van Wachem, Numerical time-step restrictions as a result of capillary waves, Journal of Computational Physics 285 (2015) 24–40. doi:10.1016/j.jcp.2015.01.021.
URL http://www.sciencedirect.com/science/article/pii/S002199911500025X
[35] M. Coquerelle, S. Glockner, A fourth-order accurate curvature computation in a level set framework for two-phase flows subjected to surface tension forces, Journal of Computational Physics 305 (2016) 838–876. doi:10.1016/j.jcp.2015.11.014.
URL http://www.sciencedirect.com/science/article/pii/S0021999115007548
[36] G. Tryggvason, Numerical simulations of the Rayleigh-Taylor instability, Journal of Computational Physics 75 (2) (1988) 253–282. doi:10.1016/0021-9991(88)90112-X.
URL https://www.sciencedirect.com/science/article/pii/002199918890112X
[37] J. L. Guermond, L. Quartapelle, A Projection FEM for Variable Density Incompressible Flows, Journal of Computational Physics 165 (1) (2000) 167–188. doi:10.1006/jcph.2000.6609.
URL https://www.sciencedirect.com/science/article/pii/S0021999100966099
[38] H. Ding, P. D. M. Spelt, C. Shu, Diffuse interface model for incompressible two-phase flows with large density ratios, Journal of Computational Physics 226 (2) (2007) 2078–2095. doi:10.1016/j.jcp.2007.06.028.
URL https://www.sciencedirect.com/science/article/pii/S0021999107002793